Covert Communications in STAR-RIS Assisted NOMA IoT Networks Over Nakagami-*m* Fading Channels

Qiang Li, *Graduate Student Member, IEEE*, Dongyang Xu, *Member, IEEE*, Keyue Zhang, Keivan Navaie, *Senior Member, IEEE*, and Zhiguo Ding, *Fellow, IEEE*

***Abstract*—The combination of simultaneously transmitting and reflecting-reconfigurable intelligent surface (STAR-RIS) and nonorthogonal multiple access (NOMA) brings the necessary full-space degrees of freedom and spatial multiplexing gains for the Internet of Things (IoT) networks. The inherent network heterogeneity and sharing of wireless channels may however increase the exposure of the information interactions to the third party. To address this issue, we propose a covert communication scheme in STAR-RIS assisted NOMA networks over Nakagami-*m* fading channels, where both downlink and uplink IoT scenarios are considered. Under the NOMA protocol with imperfect successive interference cancelation (SIC), an IoT access point interacts with two IoT users aided by a STAR-RIS without being detected by two wardens. In this scenario, the two IoT users are located on both sides of the STAR-RIS which adopts coherent phase shifting and operates according to the mode switching protocol. To evaluate the wardens' detection performance, the Kullback-Leibler (KL) divergence is used. Furthermore, the cascaded channel gains of IoT users and wardens are, respectively, characterized as Gamma and complex Gaussian random variables. The closed-form expressions of the expectations of KL divergence and the interruption probabilities for downlink and uplink are derived. To further improve the performance, we formulate the effective covert rate maximization as the joint optimization problems of the transmit power and power allocation coefficient for downlink and uplink, subject to the constraints for covertness, reliability and power budget, which are, respectively, resolved analytically. Extensive simulation results indicate that the proposed scheme improves covertness compared with the benchmarks.**

Manuscript received 17 July 2023; revised 28 February 2024; accepted 19 March 2024. Date of publication 27 March 2024; date of current version 7 June 2024. This work was supported in part by the National Key Research and Development Program of China under Grant 2022YFB2902203, and in part by the Open Research Fund of National Mobile Communications Research Laboratory, Southeast University under Grant 2023D13. *(Corresponding author: Dongyang Xu.)*

Qiang Li is with the School of Information and Communication Engineering, Xi'an Jiaotong University, Xi'an 710049, China (e-mail: liqiang16@stu.xjtu.eud.cn).

Dongyang Xu is with the School of Information and Communication Engineering, Xi'an Jiaotong University, Xi'an 710049, China, and also with the National Mobile Communications Research Laboratory, Southeast University, Nanjing 211189, China (e-mail: xudongyang@xjtu.edu.cn).

Keyue Zhang is with the School of Electronics and Information, Northwestern Polytechnical University, Xi'an 710072, China, and also with the School of Microelectronics, Xi'an Jiaotong University, Xi'an 710049, China (e-mail: keyue.zhang@nwpu.edu.cn).

Keivan Navaie is with the School of Computing and Communications, Lancaster University, LA1 4WA Lancaster, U.K. (e-mail: k.navaie@lancaster.ac.uk).

Zhiguo Ding is with the Department of Computer and Communication Engineering, Khalifa University, Abu Dhabi, UAE (e-mail: zhiguo.ding@ieee.org).

Digital Object Identifier 10.1109/JIOT.2024.3381596

***Index Terms*—Covert communications, Internet of Things (IoT), nonorthogonal multiple access (NOMA), reconfigurable intelligence surface (RIS), simultaneously transmitting and reflecting (STAR).**

I. Introduction

THE PAST decade has witnessed the revolutionary progress of the communication technologies, which is already evolving to the sixth generation (6G) wireless communication networks. The first 6G white paper, entitled "Vision of 6G wireless systems: applications, trends, technologies, and open research problems," pointed out that 6G networks would achieve high reliability, high bandwidth efficiency, high security, high transmission speed and low delay communications [1]. These features facilitate the emerging Internet of Things (IoT) applications, such as remote surgery, smart homes, intelligent transportation and smart cities, which will exponentially increase the number of IoT terminals and ubiquitous personalized services [2]. It has been predicted that there will be 75 billion IoT devices connected to the IoT networks by 2030, bringing tremendous challenges to the existing networks in terms of network performance, resources and architecture [3], [4]. Developing the multiple access techniques to support high security, sufficient coverage, and lower resource consumption communication in the IoT networks has attracted increasing attention from researchers.

Nonorthogonal multiple access (NOMA) and reconfigurable intelligent surface (RIS) have been emerged as two potential technologies to cope with the above challenges [5]. On the one hand, NOMA accommodates multiple services in parallel by serving them at different power levels via the successive interference cancelation (SIC), in favor of massive connectivity, improving spectral efficiency and reducing the transmission delay [6]. Due to these capabilities, NOMA has been widely applied in the IoT scenarios, such as massive machine type communications (mMTCs), unmanned aerial vehicle (UAV) communications and ultrareliable low-latency communications (uRLLCs) [7], [8], [9]. On the other hand, a RIS consists of a large number of passive particle metamaterial elements, each of which can independently reconfigure the properties of the incident signals, i.e., their phase and amplitude, controlled by a smart controller [10]. With extremely low cost and power consumption, RIS can improve the spatial diversity gain, expand the transmission coverage and

create favorable propagation environments for received electromagnetic waves [11]. With these strengths, RIS has been recognized as an important component in the IoT networks to improve channel capacities, save transmission costs and relay long-distance transmissions et cetera [12], [13], [14].

A. Related Works

Benefitting from these capabilities, applying the potentials of the RIS into NOMA IoT networks has recently emerged as a hot research topic. For instance, [15] and [16] characterized the reliability improvement for RIS-assisted NOMA networks. Considering the tradeoff between the sum rate and energy consumption, Wang et al. proposed an energy efficiency maximization strategy for RIS NOMA networks in [17]. By optimizing the phase of the RIS, Zou et al. [18] also proposed a machine learning-based throughput maximization scheme for RIS aided NOMA IoT networks. It is worth mentioning that the RIS requires all served users to be located on the same side of the RIS, limiting the system's degrees of freedom. To overcome this issue, the simultaneously transmitting and reflecting (STAR)-RIS was introduced. Each element of the simultaneously transmitting and reflecting-reconfigurable intelligent surface (STAR-RIS) can reflect and refract the incident signals in parallel under the protocols of power splitting, mode switching or time switching, which provides the full-space (i.e., 360°) coverage for IoT networks [19]. It was shown in [20] that the STAR-RIS could significantly extend the coverage compared with the RIS. Du et al. also proposed a wireless powered IoT transmission framework using the STAR-RIS in [21].

The combination of the STAR-RIS and NOMA IoT networks was also shown to provide further performance gain. For instance, [22] provided a general analytical framework for the STAR-RIS-based NOMA network, in which the coverage probability and average transmission rates of users were characterized. Wang et al. [23] also pointed out that the received signal-to-noise ratios (SNRs) of NOMA users were maximized when the coherent phase shifting was adopted at STAR-RIS. Liu et al. [24] analyzed the effective capacity in the STAR-RIS-based NOMA network, where the latency demands of NOMA users also were discussed. Considering the eavesdropping risk, Li et al. [25] formulated the secrecy interruption probability to evaluate the secrecy of the STAR-RIS NOMA network. As compared with the orthogonal multiple access (OMA), [26] also showed that applying the STAR-RIS into multiple-input and multiple-output (MIMO) NOMA networks could yield higher energy efficiency gains. Furthermore, [27] deployed the STAR-RIS NOMA in UAV networks, which maximized the sum rate of networks by optimizing the location of the UAV and phases of the STAR-RIS.

Owing to the openness and sharing of IoT transmission medium, the transmitted information is directly exposed to the networks. For security-sensitive contents, this is a securing risk. For instance, in unmanned remote control systems, in case they are detected and then jammed, control commands might be disrupted, resulting in the system failure. Covert communication techniques, aiming at achieving the information transmissions without being detected by malicious wardens, were introduced to remedy the vacancy. With the help of a relay, Gao et al. [28] achieved covert transmissions in IoT networks. Wang et al. [29], Tao et al. [30], Duan et al. [31], and Tao et al. [32] investigated covert communication in NOMA networks. The key idea of these existing works is to confuse the wardens by creating uncertainty by means of channel inversion power control [29], random transmit power [30], uncertain channel distribution information [31] and extra imposed jamming [32]. Such techniques intentionally increased the detection error probabilities of wardens so that wardens could not effectively tell whether the communication occurred. Liu et al. [33] utilized the Kullback-Leibler (KL) divergence to characterize the detection performance of wardens, providing a novel paradigm for covert communication design.

Recently, the covert communication in RIS IoT networks has also been extensively explored. For instance, Ma et al. [34] considered the covert transmission in RIS-assisted IoT networks, in which two covert rate maximization strategies were proposed with and without the channel state information (CSI) of the warden. Mamaghani and Hong [35] also investigated an energy-efficient covert UAV communication scheme over the terahertz (THz) band with the help of the RIS, which improved the covert throughput. Furthermore, considering the information freshness, [36] proposed an opportune two-way information exchange protocol for RIS aided networks. Considering residual hardware impairments, Chen et al. [37] maximized the network capacity under the constraint of the covertness by jointly optimizing the transmit power and the phases of the RIS for RIS IoT networks. By introducing the phase uncertainty from the RIS, [38] achieved the covert uplink and downlink transmission for RIS aided NOMA networks. Yang et al. [39] jointly considered the security and covertness for RIS assisted NOMA networks, in which the secrecy outage probability and the detection error probability were characterized.

B. Motivations and Contributions

In the above mentioned research efforts, we recognize the following significant observations.

1) In the existing literatures on covert communication in NOMA networks [29], [30], [31], [32], [38], [39], it has been assumed that there are two users in NOMA networks. One of them is a public user and the other is a covert user. Regardless of the covert action, the public user always sends information to provide a shelter. This is however resources-wasting without necessary public action. Therefore, it is necessary to investigate the covert communication of the NOMA network as a whole.
2) For an IoT node located far away from the IoT access point [28], the relay is deployed to assist the covert transmission. The relay divides the covert action into two phases, which provides warden another opportunity for the detection. Simultaneously, the increased power by the relay makes information transmission more exposed, which is damaging to remote covert action.
3) Existing approaches of covert communications focused on confusing the warden by creating uncertainty, such as power, channel and noise uncertainty [28], [29], [30],

[31], [32], [33], which might reduce the performance of legitimate transmissions and require additional transmission costs. In the STAR-RIS aided communication, the phase shifting of the elements is also a potential uncertainty source, which does not require the extra cost and design.

4) In the existing works on covert RIS transmissions [34], [35], [36], [37], [38], [39], it is required that all users are located at the same side of the RIS. This however decreases the degrees of freedom and only provides half-space covert transmission. For users on the opposite side of the RIS, covert communication is unlikely to be achieved.

Inspired by these observations, this article considers the covert communication in STAR-RIS assisted NOMA networks for downlink and uplink IoT scenarios, for the first time. Under the NOMA protocol with the imperfect SIC, an IoT access point aims at covertly completing the information interactions with two IoT users, aided by a STAR-RIS. Each of these IoT users is monitored by a warden. The two IoT users are located on both sides of the STAR-RIS. Similar to [23], the coherent phase shifting is adopted at the STAR-RIS working in the mode switching protocol, which can maximize the received SNR of IoT users. Our goal is to hide the entire interactions of STAR-RIS assisted NOMA networks. The main contributions of this article are fourfold.

1) We propose a novel covert STAR-RIS assisted NOMA transmission scheme over Nakagami-m fading channels for downlink and uplink IoT scenarios. Considering that the wardens cannot feed back their channel information, only statistical CSI of wardens is available at the IoT access point. In the scheme, the phase shifting of the STAR-RIS provides a shelter for the covert actions and the KL divergence is utilized as the metric to analyze the detection performance of wardens.
2) For the proposed scheme, we provide an analytical framework for covertness and reliability of the networks. The cascaded channel gains of the IoT users are characterized as two random variables (RVs) following Gamma distribution. The cascaded channel gain of wardens is approximated as two complex Gaussian RV. We further derive the closed-form expressions of the expectations of KL divergence and transmission interruption probabilities under the imperfect SIC for downlink and uplink IoT scenarios to evaluate the covertness and reliability of the networks.
3) In order to improve the performance, we formulate the effective covert rate (ECR) maximization problems, subject to covertness demands, reliability constraints and power boundary constraints. For the downlink IoT scenario, by jointly optimizing the transmit power and power allocation coefficient of the IoT access point, the maximum ECR is captured analytically. For the uplink IoT scenario, by joint optimizing the transmit power of two IoT users, the maximum ECR is acquired by numerical search.
4) Numerical results are presented to demonstrate that applying the potentials of the STAR-RIS into NOMA networks can bring more covertness gains, as compared with benchmarks.

TABLE I
DEFINITION OF THE ACRONYMS

Abbreviations	Descriptions
AWGN	Additive white Gaussian noise
CSI	Channel state information
IoT	Internert of Things
KL divergence	Kullback-Leibler divergence
MDEP	Minimum detection error probability
NOMA	Non-orthogonal multiple access
RIS	Reconfigurable intelligent surface
RV	Random variable
SIC	Successive interference cancellation
SNR(SINR)	Signal to (interference and) noise ratio
STAR	Simultaneously transmitting and reflecting

The rest of this article is organized as follows. Section II introduces the system and channel models for the STAR-RIS assisted NOMA networks. Section III analyzes the joint information transmissions, covertness, and covert scheme design for the downlink IoT scenarios. Section IV details the joint information transmissions, covertness and covert scheme design for the uplink IoT scenarios. Numerical results are presented in Section V. Finally, Section VI concludes this article.

Notations: The uppercase and lowercase boldface letters serve as the matrixes and vectors, respectively. $X \sim f(x)$ shows that probability density function (pdf) of X is $f(x)$. $\mathcal{CN}(a, b)$ and $\mathcal{N}(a, b)$, respectively, denote the circular symmetric complex Gaussian distribution and Gaussian distribution with mean a and variance b. $\Gamma(k, \theta)$ and $U(a, b)$, respectively, mean Gamma distribution with shape parameter k and scale parameter θ and uniform distribution over the interval (a, b). $\text{diag}(\cdot) \in \mathbb{C}^{K\times K}$ means $K \times K$ diagonal matrix. $\mathbb{E}(\cdot)$, $\mathbb{V}(\cdot)$ and $\mathbb{P}(\cdot)$, respectively, denote the expectation, variance and probability operations. Some main abbreviations used below and their descriptions are summarized in the Table I.

II. SYSTEM MODEL

As exhibited in Fig. 1, this article considers the covert communication in the STAR-RIS assisted NOMA network for the downlink and uplink IoT scenarios. The network consists of an IoT access point (Alice), two IoT users (Bob and Cindy), two wardens (Willie 1 and Willie 2) and a STAR-RIS. Wherein, Alice aims to covertly exchange the information with Bob and Cindy, by means of the NOMA protocol. According to the distance to Alice, Bob and Cindy are the near and far terminals, respectively. Due to tall obstacles, there is no direct link between Alice and Cindy. To facilitate the transmission, similar to [25], a STAR-RIS capable of both reflecting and refracting the incident signals is deployed in the networks, where Alice and Bob are located on one side of the STAR-RIS and Cindy is located on the other side of the STAR-RIS. Specifically, the STAR-RIS consists of $2K$ reconfigurable elements, each of which can reflect or refract the signals on

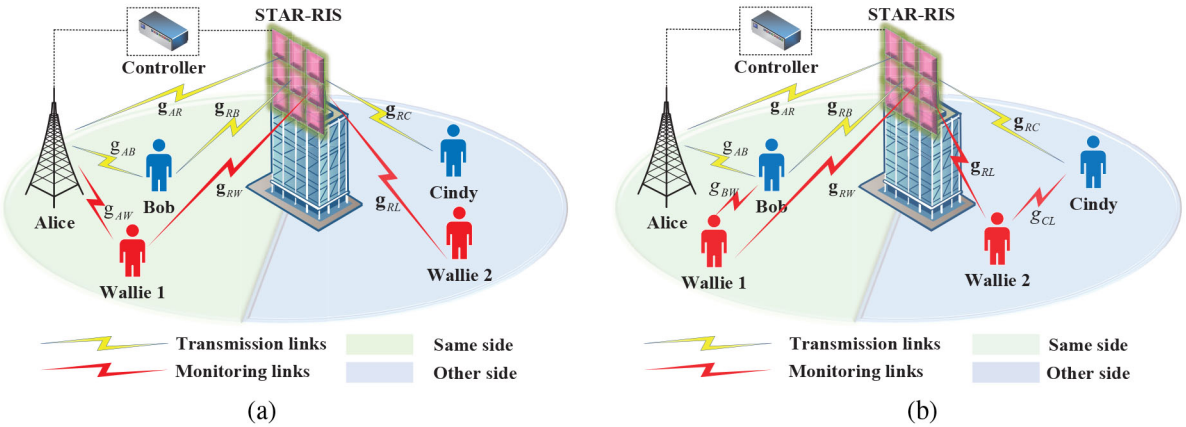

Fig. 1. System model for STAR-RIS assisted NOMA IoT networks: (a) Downlink. (b) Uplink.

its own. And the STAR-RIS is controlled by Alice through a smart controller adjusting the parameters of all elements.

Similar to [25], to facilitate deployment, it is assumed that the STAR-RIS works in the mode switching protocol and divides its $2K$ elements into two equal parts for the reflection and refraction. In addition, Willie 1 and Willie 2, who are likely to be idle IoT nodes, respectively, monitor the communication behaviors of Bob and Cindy in the network. As such, Willie 1 and Bob are located on the same side of the STAR-RIS, while Willie 2 and Cindy are located on the other side of the STAR-RIS. This article considers the overall covertness of the entire network as a whole, i.e., as long as one of Willie 1 and Willie 2 can detect communication behaviors, the covert transmissions will be suspended.

In the network, each terminal is equipped with a single antenna and works according to the half-duplex mode. Assume that the channels associated with the STAR-RIS undergo independently distributed (i.d.) Nakagami-m fading along with path loss. And the channels of direct links are captured by the Rayleigh fading along with path loss. Let d_{AB}, d_{AW}, d_{BW}, d_{CL}, d_{AR}, d_{RB}, d_{RW}, d_{RC} and d_{RL} denote the distances of links Alice $\rightarrow$ Bob, Alice $\rightarrow$ Willie 1, Bob $\rightarrow$ Willie 1, Cindy $\rightarrow$ Willie 2, Alice $\rightarrow$ STAR-RIS, STAR-RIS $\rightarrow$ Bob, STAR-RIS $\rightarrow$ Willie 1, STAR-RIS $\rightarrow$ Cindy and STAR-RIS $\rightarrow$ Willie 2, respectively. The corresponding small-scale fading coefficients are, respectively, expressed as g_{AB}, g_{AW}, g_{BW}, g_{CL}, $\mathbf{g}_{AR}$, $\mathbf{g}_{RB}$, $\mathbf{g}_{RW}$, $\mathbf{g}_{RC}$ and $\mathbf{g}_{RL}$, where $g_{AB}, g_{AW}, g_{BW}, g_{CL} \sim \mathcal{CN}(0,1)$, $\mathbf{g}_{\Delta} \in \mathbb{C}^{K\times 1}$ and $|g_{\Delta,k}| \sim Nakagami(m_{\Delta},1)$, $\Delta \in \{AR, RB, RW, RC, RL\}$, $k \in [1, K]$ and $|g_{\Delta,k}|$ means of the modulus of kth entry of $\mathbf{g}_{\Delta}$. The large-scale path loss coefficients are captured by $L_{\Upsilon} = L_0 d_{\Upsilon}^{-\beta}$, where $\Upsilon \in \{\Delta, AB, AW, BW, CL\}$, β is the path loss exponent and L_0 means the reference path loss per unit distance.

Regarding channel information, we have the following assumptions: 1) The channel condition of Bob is better than that of Cindy, which is a general assumption to implement the SIC in the NOMA network.[1] 2) Alice knows the instantaneous CSI of links Alice-Bob and Alice-RIS-users based on channel estimation. Only the statistical CSI of links related to wardens is available at Alice, because wardens cannot feed back their instantaneous CSI. 3) Channel reciprocity is hold in the networks. To support this, the network operates in the time-division duplexing mode for the downlink and uplink communications.

[1]The proposed scheme is also applicable to the scenario where Cindy has the better channel condition, which provides a general analytical framework.

III. Covert Communications in STAR-RIS Downlink NOMA Networks

Here, we consider the covert communications in STAR-RIS assisted downlink NOMA networks. First, we analyze the information transmission of the downlink NOMA networks. Then, we detail the covertness of the networks. Finally, the covert transmission scheme is designed.

A. STAR-RIS Assisted Downlink NOMA Transmissions

As shown in Fig. 1(a), in the downlink NOMA networks, Alice transmits two unit-power covert signals x_B and x_C to Bob and Cindy with the help of a STAR-RIS, respectively. The received signals at Bob and Cindy can be denoted by

$$y_B[m] = \left(\sqrt{L_{AB}}g_{AB} + \sqrt{L_{AR}L_{RB}}\mathbf{g}_{RB}^H \mathbf{\Theta}_R \mathbf{g}_{AR}\right) \times \left(\sqrt{a_1 P_A}x_B[m] + \sqrt{a_2 P_A}x_C[m]\right) + n_B[m] \quad (1)$$

and

$$y_C[m] = \sqrt{L_{AR}L_{RB}}\mathbf{g}_{RC}^H \mathbf{\Theta}_T \mathbf{g}_{AR} \times \left(\sqrt{a_1 P_A}x_B[m] + \sqrt{a_2 P_A}x_C[m]\right) + n_C[m] \quad (2)$$

where P_A is the transmit power at Alice. a_1 and a_2 ($a_1 + a_2 = 1$) are the power allocation factors of Alice. Bob has better channel condition, so $0 < a_1 < 0.5$. Furthermore, $n_B \sim \mathcal{CN}(0, \sigma_B^2)$ and $n_C \sim \mathcal{CN}(0, \sigma_C^2)$ are the additive white Gaussian noises (AWGNs) at Bob and Cindy, respectively. m is the index of channel use for the occupied slot. $\mathbf{\Theta}_R = \text{diag}(e^{j\theta_1^R}, \ldots, e^{j\theta_k^R}, \ldots, e^{j\theta_K^R}) \in \mathbb{C}^{K\times K}$ and $\mathbf{\Theta}_T = \text{diag}(e^{j\theta_1^T}, \ldots, e^{j\theta_k^T}, \ldots, e^{j\theta_K^T}) \in \mathbb{C}^{K\times K}$ denote the reflection and refraction coefficients matrixes with $\theta_k^R, \theta_k^T \in [0, 2\pi)$ being the phase shift of kth element of the STAR-RIS regulated by Alice.

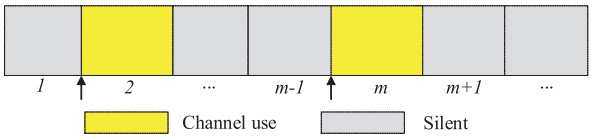

Fig. 2. Channel use diagram of the selected transmission slot.

In the NOMA network, Bob first decodes x_C and then extracts x_B by removing the partial x_C. Considering the imperfect SIC, the signal to interference and noise ratio (SINR) extracting x_C and SNR decoding x_B at Bob can be given by

$$\gamma_{B,C} = \frac{\left|\sqrt{L_{AB}}g_{AB} + \sqrt{L_{AR}L_{RB}}\mathbf{g}_{RB}^H\mathbf{\Theta}_R\mathbf{g}_{AR}\right|^2 a_2 P_A}{\left|\sqrt{L_{AB}}g_{AB} + \sqrt{L_{AR}L_{RB}}\mathbf{g}_{RB}^H\mathbf{\Theta}_R\mathbf{g}_{AR}\right|^2 a_1 P_A + \sigma_B^2} \tag{3}$$

and

$$\gamma_B = \frac{\left|\sqrt{L_{AB}}g_{AB} + \sqrt{L_{AR}L_{RB}}\mathbf{g}_{RB}^H\mathbf{\Theta}_R\mathbf{g}_{AR}\right|^2 a_1 P_A}{\phi\left|\sqrt{L_{AB}}g_{AB} + \sqrt{L_{AR}L_{RB}}\mathbf{g}_{RB}^H\mathbf{\Theta}_R\mathbf{g}_{AR}\right|^2 a_2 P_A + \sigma_B^2} \tag{4}$$

respectively, where $0 \leq \phi < 1$ is the imperfect SIC factor with $\phi = 0$ meaning the perfect SIC. Regarding x_B as the interference, the SINR of Cindy directly decoding x_C can be given by

$$\gamma_C = \frac{\left|\sqrt{L_{AR}L_{RC}}\mathbf{g}_{RC}^H\mathbf{\Theta}_T\mathbf{g}_{AR}\right|^2 a_2 P_A}{\left|\sqrt{L_{AR}L_{RC}}\mathbf{g}_{RC}^H\mathbf{\Theta}_T\mathbf{g}_{AR}\right|^2 a_1 P_A + \sigma_C^2}. \tag{5}$$

Having no access to instantaneous CSI of wardens, Alice regulates $\mathbf{\Theta}_R$ and $\mathbf{\Theta}_T$ in line with the channel information of users. As pointed out in [22], a coherent phase shifting strategy can maximize the SINR of both users. In this case, the optimal θ_k^R and θ_k^T can be, respectively, given by

$$\left(\theta_k^R\right)^* = \theta_{AB} - \left(\theta_{RB,k} + \theta_{AR,k}\right) \tag{6}$$

and

$$\left(\theta_k^T\right)^* = -\left(\theta_{RC,k} + \theta_{AR,k}\right) \tag{7}$$

where θ_{AB} and $\theta_{\Delta,k}$ denote the phases of g_{AB} and kth entry of $\mathbf{g}_\Delta$, respectively. Therefore, the optimal reflection and refraction coefficients matrixes can be, respectively, given by

$$\mathbf{\Theta}_R^* = \mathrm{diag}\left(e^{j(\theta_1^R)^*}, \ldots, e^{j(\theta_k^R)^*}, \ldots, e^{j(\theta_K^R)^*}\right) \tag{8}$$

and

$$\mathbf{\Theta}_T^* = \mathrm{diag}\left(e^{j(\theta_1^T)^*}, \ldots, e^{j(\theta_k^T)^*}, \ldots, e^{j(\theta_K^T)^*}\right). \tag{9}$$

B. Covertness Analysis of STAR-RIS Downlink NOMA

1) Detection at Wardens: To avoid being detected by wardens, Alice cannot always transmit the signals in each slot. As shown in Fig. 2, Alice sends the covert information with a certain prior probability ρ in a selected slot. As such, the wardens remain uncertain on whether the covert signals are sent. They need to make a binary judgement in line with their observations in the network. Let $\mathcal{H}0$ and $\mathcal{H}1$ denote, respectively, the two hypnoses that Alice sends and does not send the covert signals to NOMA users. Therefore, the received signals at Willie 1 and Willie 2 can be given as follows:

$$\begin{cases} \mathcal{H}0: y_{W1}[m] = n_{W1}[m] \\ \mathcal{H}0: y_{W2}[m] = n_{W2}[m] \\ \mathcal{H}1: y_{W1}[m] = \left(\sqrt{L_{AW}}g_{AW} + \sqrt{L_{AR}L_{RW}}\mathbf{g}_{RW}^H\mathbf{\Theta}_R\mathbf{g}_{AR}\right) \\ \times\left(\sqrt{a_1 P_A}x_B[m] + \sqrt{a_2 P_A}x_C[m]\right) + n_{W1}[m] \\ \mathcal{H}1: y_{W2}[m] = \sqrt{L_{AR}L_{RL}}\mathbf{g}_{RL}^H\mathbf{\Theta}_T\mathbf{g}_{AR} \\ \times\left(\sqrt{a_1 P_A}x_B[m] + \sqrt{a_2 P_A}x_C[m]\right) + n_{W2}[m] \end{cases} \tag{10}$$

where, $n_{W1} \sim \mathcal{CN}(0, \sigma_{W1}^2)$ and $n_{W2} \sim \mathcal{CN}(0, \sigma_{W2}^2)$ denote the AWGN at Willie 1 and Willie 2, respectively. In (10), m is the index of channel use for the occupied slot. Without loss of generality, $\sigma_B^2 = \sigma_C^2 = \sigma_0^2$ and $\sigma_{W1}^2 = \sigma_{W2}^2 = \sigma_W^2$ are set. Assume that Alice chooses to send covert signals or not with an equal prior probability, i.e., $\rho = 0.5$. To maximize the detection performance, the wardens adopt the optimal test strategy. The corresponding minimum detection error probability (MDEP) can be computed by [33]

$$\Xi^* = 1 - \mathcal{V}_T\left(\mathbb{P}_0^{W1/W2}, \mathbb{P}_1^{W1/W2}\right) \tag{11}$$

where $\mathcal{V}_T(\mathbb{P}_0^{W1/W2}, \mathbb{P}_1^{W1/W2})$ is the total variation distance between $\mathbb{P}_0^{W1/W2}$ and $\mathbb{P}_1^{W1/W2}$ being the probability distributions of received signals at Willie 1/Willie 2 under $\mathcal{H}0$ and $\mathcal{H}1$ shown as follows: $\mathbb{P}_0^{W1} \triangleq f(y_{W1}[m]|\mathcal{H}0) = \mathcal{CN}(0, \sigma_W^2)$, $\mathbb{P}_0^{W2} \triangleq f(y_{W2}[m]|\mathcal{H}0) = \mathcal{CN}(0, \sigma_W^2)$, $\mathbb{P}_1^{W1} \triangleq f(y_{W1}[m]|\mathcal{H}1) = \mathcal{CN}(0, P_A|\sqrt{L_{AW}}g_{AW} + \sqrt{L_{AR}L_{RW}}\mathbf{g}_{RW}^H\mathbf{\Theta}_R\mathbf{g}_{AR}|^2 + \sigma_W^2)$ and $\mathbb{P}_1^{W2} \triangleq f(y_{W2}[m]|\mathcal{H}1) = \mathcal{CN}(0, P_A|\sqrt{L_{AR}L_{RL}}\mathbf{g}_{RL}^H\mathbf{\Theta}_T\mathbf{g}_{AR}|^2 + \sigma_W^2)$. Since $\mathcal{V}_T(\mathbb{P}_0^{W1/W2}, \mathbb{P}_1^{W1/W2})$ is difficult to handle, by the Pinsker's inequality [33], a tractable upper bound is obtained as

$$\mathcal{V}_T\left(\mathbb{P}_0^{W1/W2}, \mathbb{P}_1^{W1/W2}\right) \leq \sqrt{0.5\mathcal{D}\left(\mathbb{P}_0^{W1/W2}\|\mathbb{P}_1^{W1/W2}\right)} \tag{12}$$

where $\mathcal{D}(\mathbb{P}_0^{W1/W2}\|\mathbb{P}_1^{W1/W2})$ is the KL divergence from $\mathbb{P}_0^{W1/W2}$ to $\mathbb{P}_1^{W1/W2}$, which can be, respectively, calculated by

$$\begin{aligned} \mathcal{D}_{W1} &= \mathcal{D}\left(\mathbb{P}_0^{W1}\|\mathbb{P}_1^{W1}\right) \\ &= \int_x f(y_{W1}(x)[m]|\mathcal{H}0)\ln\frac{f(y_{W1}(x)[m]|\mathcal{H}0)}{f(y_{W1}(x)[m]|\mathcal{H}1)}dx \\ &\overset{(a)}{=} \ln\left(1 + \frac{\sigma_{\nu_1}^2}{\sigma_W^2}\right) + \frac{\sigma_W^2}{\sigma_{\nu_1}^2 + \sigma_W^2} - 1 \end{aligned} \tag{13}$$

and

$$\begin{aligned} \mathcal{D}_{W2} &= \mathcal{D}\left(\mathbb{P}_0^{W2}\|\mathbb{P}_1^{W2}\right) \\ &= \int_x f(y_{W2}(x)[m]|\mathcal{H}0)\ln\frac{f(y_{W2}(x)[m]|\mathcal{H}0)}{f(y_{W2}(x)[m]|\mathcal{H}1)}dx \\ &\overset{(a)}{=} \ln\left(1 + \frac{\sigma_{\nu_2}^2}{\sigma_W^2}\right) + \frac{\sigma_W^2}{\sigma_{\nu_2}^2 + \sigma_W^2} - 1 \end{aligned} \tag{14}$$

where (a) is obtained by substituting the expressions of the probability distributions into the integral. $\sigma_{\nu_1}^2$ and $\sigma_{\nu_2}^2$ is, respectively, given by

$$\sigma_{\nu_1}^2 = P_A\left|\sqrt{L_{AW}}g_{AW} + \sqrt{L_{AR}L_{RW}}\mathbf{g}_{RW}^H\mathbf{\Theta}_R\mathbf{g}_{AR}\right|^2 \tag{15}$$

and

$$\sigma_{\nu_2}^2 = P_A \left| \sqrt{L_{AR} L_{RL}} \mathbf{g}_{RL}^H \mathbf{\Theta}_T \mathbf{g}_{AR} \right|^2. \quad (16)$$

Substituting (12) into (11) indicates the MDEP satisfies

$$\Xi^* \geq 1 - \sqrt{0.5 \mathcal{D}\left(\mathbb{P}_0^{W1/W2} \| \mathbb{P}_1^{W1/W2} \right)}. \quad (17)$$

Generally, covert communication is achieved when $\Xi^* \geq 1-\varepsilon$, where $\varepsilon > 0$ being an arbitrarily small value represents the level of covertness. Therefore, the covertness constraint (17) can be rewritten as

$$\mathcal{D}\left(\mathbb{P}_0^{W1/W2} \| \mathbb{P}_1^{W1/W2} \right) \leq 2\varepsilon^2. \quad (18)$$

2) Expected Detection Performance: Having no access to the instantaneous CSI related to wardens, Alice is unaware of the values of $\sigma_{\nu_2}^1$ and $\sigma_{\nu_2}^2$. Here, we utilize the expected values of $\mathcal{D}(\mathbb{P}_0^{W1/W2} \| \mathbb{P}_1^{W1/W2})$ over all channel realizations of wardens to evaluate covertness of the networks.

Lemma 1: For a sufficiently large K, $\xi_W = \mathbf{g}_{RW}^H \mathbf{\Theta}_R \mathbf{g}_{AR}$ can be approximated as a circularly symmetric complex Gaussian RV with mean 0 and variance K, i.e.,

$$\xi_{AW} = \mathbf{g}_{RW}^H \mathbf{\Theta}_R \mathbf{g}_{AR} \sim \mathcal{CN}(0, K). \quad (19)$$

Proof: Given the optimal reflection coefficients matrix $\mathbf{\Theta}_R^*$ of the STAR-RIS, ξ_W can be rewritten as

$$\begin{aligned} \xi_{AW} &= \mathbf{g}_{RW}^H \mathbf{\Theta}_R \mathbf{g}_{AR} \\ &= \sum_{k=1}^{K} |g_{RW,k}||g_{AR,k}| e^{j\left(\theta_{RW,k} + \theta_{AR,k} + (\theta_k^R)^*\right)} \\ &= \sum_{k=1}^{K} |g_{RW,k}||g_{AR,k}| e^{j(\theta_{RW,k} + \theta_{AB} - \theta_{RB,k})} \end{aligned} \quad (20)$$

which is the sum of K out-of-phase complex-valued coefficients. Note that wardens have no access to the working mode and the phase shifting of the STAR-RIS. Therefore, under the uplink channel estimation, $\theta_{RW,k}$, θ_{AB} and $\theta_{RB,k}$ are i.i.d. RVs uniformly distributed on the interval $[0, 2\pi)$, and their weighted sum also follows the same uniform distribution $U[0, 2\pi)$ for wardens. In the light of the central limit theorem (CLT) [16], ξ_W can be approximated as a 0-mean complex Gaussian RV. By means of [15, Lemma 4] and Appendix C in [16], the probability distribution of ξ_{AW} can be obtained for a sufficiently large K. We note that in [16] it was shown that the approximation is tight even for a relatively small K. ■

Lemma 2: For a sufficiently large K, $\xi_L = \mathbf{g}_{RL}^H \mathbf{\Theta}_T \mathbf{g}_{AR}$ can be approximated as a circularly-symmetric complex Gaussian RV with mean 0 and variance K, i.e.,

$$\xi_{AL} = \mathbf{g}_{RL}^H \mathbf{\Theta}_T \mathbf{g}_{AR} \sim \mathcal{CN}(0, K). \quad (21)$$

Proof: Similar to the proof of Lemma 1. ■

According to Lemma 1, $\sigma_{\nu_1}^2$ can be reconstructed as

$$\begin{aligned} \sigma_{\nu_1}^2 &= P_A \left| \sqrt{L_{AW}} g_{AW} + \sqrt{L_{AR} L_{RW}} \mathbf{g}_{RW}^H \mathbf{\Theta}_R \mathbf{g}_{AR} \right|^2 \\ &= P_A (L_{AW} + K L_{AR} L_{RW}) |\xi_0|^2 \end{aligned} \quad (22)$$

where $\xi_0 \sim \mathcal{CN}(0, 1)$. As such, $\sigma_{\nu_1}^2$ can be regarded as an exponential RV with expectation $\lambda_{W1} = P_A(L_{AW} + K L_{AR} L_{RW})$, i.e.,

$$\sigma_{\nu_1}^2 \sim \exp\left(\frac{1}{\lambda_{W1}} \right) = \exp\left(\frac{1}{P_A (L_{AW} + K L_{AR} L_{RW})} \right). \quad (23)$$

Similarly, according to Lemma 2, $\sigma_{\nu_2}^2$ can be regarded as an exponential RV and its pdf is given by

$$\sigma_{\nu_2}^2 \sim \exp\left(\frac{1}{\lambda_{W2}} \right) = \exp\left(\frac{1}{P_A K L_{AR} L_{RL}} \right). \quad (24)$$

Based on the above analysis, in the following theorems, we derive the expected values of $\mathcal{D}(\mathbb{P}_0^{W1/W2} \| \mathbb{P}_1^{W1/W2})$ over all channel realizations.

Theorem 1: The expected value of $\mathcal{D}(\mathbb{P}_0^{W1} \| \mathbb{P}_1^{W1})$ over all realization of $\sigma_{\nu_1}^2$ can be calculated as

$$\mathcal{E}_{W1} = -\left(1 + \frac{\sigma_W^2}{\lambda_{W1}} \right) \exp\left(\frac{\sigma_W^2}{\lambda_{W1}} \right) \mathrm{Ei}\left(-\frac{\sigma_W^2}{\lambda_{W1}} \right) - 1 \quad (25)$$

where $\mathrm{Ei}(x) = \int_{-\infty}^{x} e^t/t dt$ is the exponential integral function [40, eq. (8.211)].

Proof: For $x \geq 0$, the pdf of $\sigma_{\nu_1}^2$ is expressed as $f_{\sigma_{\nu_1}^2}(x) = (1/\lambda_{W1}) \exp[-(1/\lambda_{W1})x]$. Therefore, $\mathcal{E}_{W1}$ can be given by

$$\begin{aligned} \mathcal{E}_{W1} &= \mathbb{E}\left(\mathcal{D}\left(\mathbb{P}_0^{W1} \| \mathbb{P}_1^{W1} \right) \right) \\ &= \underbrace{\int_0^{\infty} \ln\left(1 + \frac{x}{\sigma_W^2} \right) f_{\sigma_{\nu_1}^2}(x) dx}_{\mathcal{E}_{11}} + \underbrace{\int_0^{\infty} \frac{\sigma_W^2 f_{\sigma_{\nu_1}^2}(x)}{x + \sigma_W^2} dx}_{\mathcal{E}_{12}} - 1 \end{aligned} \quad (26)$$

where

$$\begin{aligned} \mathcal{E}_{11} &= \int_0^{\infty} \ln\left(1 + \frac{x}{\sigma_W^2} \right) \frac{1}{\lambda_{W1}} \exp\left(-\frac{1}{\lambda_{W1}} x \right) dx \\ &\overset{(b)}{=} -\exp\left(\frac{\sigma_W^2}{\lambda_{W1}} \right) \mathrm{Ei}\left(-\frac{\sigma_W^2}{\lambda_{W1}} \right) \end{aligned} \quad (27)$$

and

$$\begin{aligned} \mathcal{E}_{12} &= \int_0^{\infty} \frac{\sigma_W^2}{x + \sigma_W^2} \frac{1}{\lambda_{W1}} \exp\left(-\frac{1}{\lambda_{W1}} x \right) dx \\ &\overset{(c)}{=} -\frac{\sigma_W^2}{\lambda_{W1}} \exp\left(\frac{\sigma_W^2}{\lambda_{W1}} \right) \mathrm{Ei}\left(-\frac{\sigma_W^2}{\lambda_{W1}} \right) \end{aligned} \quad (28)$$

in which [40, eq. (4.337-2)] and [40, eq. (3.352-4)] are utilized at (b) and (c), respectively. Substituting (27) and (28) into (26), the closed-form expression of $\mathcal{E}_{W1}$ is derived and the proof is complete. ■

Theorem 2: The expected value of $\mathcal{D}(\mathbb{P}_0^{W2} \| \mathbb{P}_1^{W2})$ over all realization of $\sigma_{\nu_2}^2$ can be calculated as

$$\mathcal{E}_{W2} = -\left(1 + \frac{\sigma_W^2}{\lambda_{W2}} \right) \exp\left(\frac{\sigma_W^2}{\lambda_{W2}} \right) \mathrm{Ei}\left(-\frac{\sigma_W^2}{\lambda_{W2}} \right) - 1. \quad (29)$$

Proof: Similar to the proof of Theorem 1. ■

Using Theorems 1 and 2, in the following, the covertness of the STAR-RIS assisted downlink NOMA networks can be evaluated through the constraints:

$$\mathcal{E}_{W1} \leq 2\varepsilon^2, \quad \text{and} \quad \mathcal{E}_{W2} \leq 2\varepsilon^2. \tag{30}$$

C. Covert STAR-RIS Downlink NOMA Design

In this section, we first analyze the reliability of STAR-RIS assisted downlink NOMA networks. Then, an ECR maximization problem is formulated, subject to the covertness and reliability constraints. By solving this, the optimal system parameters can be obtained.

1) Reliability Analysis: According to the coherent phase shifting shown in (8) and (9), the cascaded channels of Bob and Cindy can be, respectively, rewritten as

$$\begin{aligned}\xi_B &= \sqrt{L_{AB}} g_{AB} + \sqrt{L_{AR}L_{RB}} \mathbf{g}_{RB}^H \mathbf{\Theta}_R \mathbf{g}_{AR} \\ &= \sqrt{L_{AB}}|g_{AB}| + \sqrt{L_{AR}L_{RB}} \sum_{k=1}^{K} |g_{AR}||g_{RB}|\end{aligned} \tag{31}$$

and

$$\begin{aligned}\xi_C &= \sqrt{L_{AR}L_{RC}} \mathbf{g}_{RC}^H \mathbf{\Theta}_T \mathbf{g}_{AR} \\ &= \sqrt{L_{AR}L_{RC}} \sum_{k=1}^{K} |g_{AR}||g_{RC}|.\end{aligned} \tag{32}$$

In the following, we analyze the distributions of the cascaded channels.

Lemma 3: For a sufficiently large K, $|\xi_B|^2$ can be approximated as a Gamma RV with the shape k_B and the scale θ_B, i.e.,

$$|\xi_B|^2 \sim \Gamma(k_B, \theta_B) \tag{33}$$

where $k_B = [(K\mu_B^2)/(4\delta_B^2)]$, $\theta_B = 4K\delta_B^2$, $\mu_B = \sqrt{[(L_{AB}\pi)/(2K^2)]} + \sqrt{L_{AR}L_{RB}}\Omega_{m_{AB}}$, $\delta_B^2 = [(L_{AB}(4-\pi))/(2K^2)] + L_{AR}L_{RB}(1 - \Omega_{m_{AB}}^2)$ and $\Omega_{m_{AB}} = [(\Gamma[m_{AR} + (1/2)]\Gamma[m_{RB} + (1/2)])/(\Gamma(m_{AR})\Gamma(m_{RB})(m_{AR}m_{RB})^{1/2})]$.

Proof: See Appendix A. ∎

Lemma 4: For a sufficiently large K, $|\xi_C|^2$ can be approximated as a Gamma RV with the shape k_C and the scale θ_C, i.e.,

$$|\xi_C|^2 \sim \Gamma(k_C, \theta_C) \tag{34}$$

where $k_C = [(K\mu_C^2)/(4\delta_C^2)]$, $\theta_C = 4K\delta_C^2$, $\mu_C = \sqrt{L_{AR}L_{RC}}\Omega_{m_{AC}}$, $\delta_C^2 = L_{AR}L_{RC}(1 - \Omega_{m_{AC}}^2)$ and $\Omega_{m_{AC}} = [(\Gamma[m_{AR} + (1/2)]\Gamma[m_{RC} + (1/2)])/(\Gamma(m_{AR})\Gamma(m_{RC})(m_{AR}m_{RC})^{1/2})]$.

Proof: See Appendix B. ∎

The approximation is shown to be tight even if $K = 4$ in [22]. In cases where the decoding SINR or SNR at terminals is less than target values, the information transmissions will be interrupted in the STAR-RIS assisted downlink network. To guarantee the reliability of covert communications, the interruption probability should be suppressed within a small range. Assume that the target rates of Bob and Cindy are R_B and R_C, respectively. In the following, we analyze the interruption probabilities of Bob and Cindy in detail.

Theorem 3: The interruption probability decoding x_B at Bob under the imperfect SIC can be given by

$$\begin{aligned}\mathcal{P}_B = 1 - &\left(1 - \frac{1}{\Gamma(k_B)}\gamma\left(k_B, \frac{\sigma_0^2 r_C}{\theta_B(a_2 - a_1 r_C)P_A}\right)\right) \\ &\times \left(1 - \frac{1}{\Gamma(k_B)}\gamma\left(k_B, \frac{\sigma_0^2 r_B}{\theta_B(a_1 - \phi a_2 r_B)P_A}\right)\right)\end{aligned} \tag{35}$$

where $r_B = 2^{R_B} - 1$ and $r_C = 2^{R_C} - 1$. $\Gamma(x) = \int_0^\infty e^{-t}t^{x-1}dt$ and $\gamma(a, x) = \int_0^x e^{-t}t^{a-1}dt$ are the gamma function [40, eq. (8.310-1)] and the lower incomplete gamma function [40, eq. (8.350-1)], respectively.

Proof: See Appendix C. ∎

Theorem 4: The interruption probability decoding x_C at Cindy can be given by

$$\mathcal{P}_C = \frac{1}{\Gamma(k_C)}\gamma\left(k_C, \frac{\sigma_0^2 r_C}{\theta_C(a_2 - a_1 r_C)P_A}\right). \tag{36}$$

Proof: See Appendix D. ∎

2) Covert Transmission Principle: In the downlink network, Alice aims to transmit two covert signals to Bob and Cindy under the help of the STAR-RIS without being detected by wardens. The ECR of the downlink network can be defined as $C_{\text{cov}}^D = (1 - \mathcal{P}_B)R_B + (1 - \mathcal{P}_C)R_C$. To improve the covert performance of the STAR-RIS assisted downlink NOMA network, we maximize the ECR of the network by jointly optimizing the transmit power P_A and power allocation coefficient a_1, subject to the reliability constraints of Bob and Cindy, the covertness constraints of the network and the boundary constraints. As such, the optimization problem can be formulated as follows:

$$\max_{a_1, P_A} \quad C_{\text{cov}}^D = (1 - \mathcal{P}_B)R_B + (1 - \mathcal{P}_C)R_C \tag{37a}$$

$$\text{s.t.} \quad \mathcal{E}_{W1} \leq 2\varepsilon^2 \tag{37b}$$

$$\mathcal{E}_{W2} \leq 2\varepsilon^2 \tag{37c}$$

$$\mathcal{P}_B \leq p_B \tag{37d}$$

$$\mathcal{P}_C \leq p_C \tag{37e}$$

$$0 < a_1 < 0.5, \text{ and } a1 + a2 = 1 \tag{37f}$$

$$0 < P_A \leq p_{\max} \tag{37g}$$

where (37b) and (37c) are the covertness constraints of the network. Equations (37d) and (37e) are the reliability constraints with p_B and p_C being the tolerable maximum interruption probabilities at Bob and Cindy, respectively. Also, (37f) and (37g) are the boundary constraints of a_1 and P_A, respectively, and $p_{\max}$ is the maximum transmit power at Alice. Since $[(d\gamma(a, x))/(dx)] = x^{a-1}e^{-x} > 0$, it is easy to show that $\mathcal{P}_B$ and $\mathcal{P}_C$ are two monotonically decreasing functions w.r.t. P_A. The ECR $\mathcal{C}_{\text{cov}}^D$ is a monotonically increasing function w.r.t. P_A. As such, the value of P_A should be as large as possible. Note that $\mathcal{E}_{W1}, \mathcal{E}_{W2}$ are only related to P_A but not to a_1. We analyze the monotonicity of $\mathcal{E}_{W1}, \mathcal{E}_{W2}$ on P_A in the following.

Lemma 5: $\mathcal{E}_{W1}, \mathcal{E}_{W2}$ are two monotonically increasing functions w.r.t. P_A.

Proof: See Appendix E. ∎

In the light of Lemma 5, (37b) and (37c) can be rewritten as $P_A \le P_A^{\dagger}$ and $P_A \le P_A^{\ddagger}$ with $P_A^{\dagger}$ and $P_A^{\ddagger}$ being the solutions of $\mathcal{E}_{W1}(P_A) = 2\varepsilon^2$ and $\mathcal{E}_{W2}(P_A) = 2\varepsilon^2$, respectively. The Larger P_A, the smaller the interruption probabilities and the larger the ECR. The optimal value P_A is determined by the covertness constraints

$$P_A^* = \min\left(p_{\max}, P_A^{\dagger}, P_A^{\ddagger}\right). \tag{38}$$

For given optimal P_A, the optimization problem (37) can be reformulated as

$$\begin{aligned} \min_{a_1} \quad & C_{cov,1}^D = \mathcal{P}_B R_B + \mathcal{P}_C R_C \\ \text{s.t.} \quad & (37d)-(37f). \end{aligned} \tag{39}$$

Note that $\mathcal{P}_C$ is a monotonically increasing function of a_1, hence (37e) can be rewritten as $a_1 \le a_1^{\dagger}$ with $a_1^{\dagger}$ being the solution of $\mathcal{P}_C(a_1) = p_C$. Also, (37e) and (37f) are jointly equivalent to $0 < a_1 \le \min(a_1^{\dagger}, 0.5)$ and $a_1 + a_2 = 1$. Owing to the complicated expressions of (35) and $C_{cov,1}^D$, it is difficult to derive their derivatives w.r.t. a_1, which is required by the Lagrange duality method. Instead, (39) can be solved by a 1-D numerical search over the interval $(0, \min(a_1^{\dagger}, 0.5))$ efficiently. Substituting the optimal a_1^* and P_A^* into C_{cov}^D, the maximum ECR of the downlink network is then obtained.

IV. Covert Communications in STAR-RIS Uplink NOMA Networks

In this section, we consider the covert communications in the STAR-RIS assisted uplink NOMA networks. First, we analyze the information transmission of the uplink NOMA networks. We then detail the covertness of the networks and design a covert transmission scheme.

A. STAR-RIS Assisted Uplink NOMA Transmissions

As shown in Fig. 1(b), in the uplink NOMA network, Bob and Cindy transmit two unit-power covert signals x_B and x_C with the help of a STAR-RIS. The received signals by Alice can be denoted by

$$\begin{aligned} y_A[m] = & \left(\sqrt{L_{AB}} g_{AB} + \sqrt{L_{AR}L_{RB}}\mathbf{g}_{AR}^H \boldsymbol{\Theta}_R' \mathbf{g}_{RB}\right) \\ & \times \sqrt{P_B} x_B[m] + \sqrt{L_{AR}L_{RB}P_C}\mathbf{g}_{AR}^H \boldsymbol{\Theta}_T' \mathbf{g}_{RC} x_C[m] \\ & + n_A[m] \end{aligned} \tag{40}$$

where P_B and P_C are the transmit powers at Bob and Cindy, respectively. Assume that the channel between Bob and Alice is better than that between Cindy and Alice, so the signal of Cindy can be allocated more power, i.e., $P_C > P_B$. Also, $n_A \sim \mathcal{CN}(0, \sigma_0^2)$ is the AWGN at Alice. $\boldsymbol{\Theta}_R' = \text{diag}(e^{j\theta_1'^R}, \ldots, e^{j\theta_k'^R}, \ldots, e^{j\theta_K'^R}) \in \mathbb{C}^{K\times K}$ and $\boldsymbol{\Theta}_T' = \text{diag}(e^{j\theta_1'^T}, \ldots, e^{j\theta_k'^T}, \ldots, e^{j\theta_K'^T}) \in \mathbb{C}^{K\times K}$ denote the reflection and refraction coefficients matrixes of the STAR-RIS in the uplink NOMA networks. Similar to the downlink NOMA networks, a coherent phase shift strategy is performed at the STAR-RIS [22]. Because of the channel reciprocity, the optimal reflection and refraction coefficients matrixes can be given by

$$\boldsymbol{\Theta}_R'^* = \boldsymbol{\Theta}_R^* \text{ and } \boldsymbol{\Theta}_T'^* = \boldsymbol{\Theta}_T^*. \tag{41}$$

Therefore, the cascaded channels between Alice and users in the uplink NOMA networks are the same as those in downlink NOMA network in Section III. We denote the cascaded channels from Bob to Alice and from Cindy to Alice by $\xi_B = \sqrt{L_{AB}} g_{AB} + \sqrt{L_{AR}L_{RB}}\mathbf{g}_{AR}^H \boldsymbol{\Theta}_R' \mathbf{g}_{RB}$ and $\xi_C = \sqrt{L_{AR}L_{RC}}\mathbf{g}_{AR}^H \boldsymbol{\Theta}_T' \mathbf{g}_{RC}$. Considering the imperfect SIC, Alice first decodes the signal of Cindy x_C by regarding the signal of Bob x_B as the interference, and then extracts the signal of Bob x_B by removing the partial x_C. The SINR decoding x_C and SINR extracting x_B by Alice can be denoted by

$$\gamma_{A,C} = \frac{|\xi_C|^2 P_C}{|\xi_B|^2 P_B + \sigma_0^2} \tag{42}$$

and

$$\gamma_{A,B} = \frac{|\xi_B|^2 P_B}{\varphi |\xi_C|^2 P_C + \sigma_0^2} \tag{43}$$

respectively, where $0 \le \varphi < 1$ is the imperfect SIC factor at Alice with $\varphi = 0$ indicating the perfect SIC.

B. Covertness Analysis of STAR-RIS Uplink NOMA

1) Detection at Wardens: In the STAR-RIS assisted uplink NOMA networks, Willie 1 and Willie 2 monitor the transmission behaviors of Bob and Cindy, respectively. As long as one of two wardens detects transmission, the communication is exposed. Assume that the transmissions by Bob and Cindy are synchronized through the synchronization frame command interaction. In a given slot, Bob and Cindy send the covert information with an equal prior probability $\rho = 0.5$. The wardens need to judge whether Bob and Cindy transmit the covert signals based on their observations. Let $\mathcal{H}_0'$ and $\mathcal{H}_1'$ represent that Bob and Cindy send the covet messages or not, respectively. Given $\mathcal{H}_0'$ and $\mathcal{H}_1'$, the received signals at Willie 1 and Willie 2 can be given as follows:

$$\begin{cases} \mathcal{H}0' : y_{W1}'[m] = n_{W1}'[m] \\ \mathcal{H}0' : y_{W2}'[m] = n_{W2}'[m] \\ \mathcal{H}1' : y_{W1}'[m] = \sqrt{L_{RW}L_{RC}P_C}\mathbf{g}_{RW}^H \boldsymbol{\Theta}_T' \mathbf{g}_{RC} x_C[m] \\ \qquad + \left(\sqrt{L_{BW}} g_{BW} + \sqrt{L_{RW}L_{RB}}\mathbf{g}_{RW}^H \boldsymbol{\Theta}_R' \mathbf{g}_{RB}\right) \\ \qquad \times \sqrt{P_B} x_B[m] + n_{W1}'[m] \\ \mathcal{H}1' : y_{W2}'[m] = \sqrt{L_{RL}L_{RB}P_B}\mathbf{g}_{RL}^H \boldsymbol{\Theta}_T' \mathbf{g}_{RB} x_B[m] \\ \qquad + \left(\sqrt{L_{CL}} g_{CL} + \sqrt{L_{RL}L_{RC}}\mathbf{g}_{RL}^H \boldsymbol{\Theta}_R' \mathbf{g}_{RC}\right) \\ \qquad \times \sqrt{P_C} x_C[m] + n_{W2}'[m]. \end{cases} \tag{44}$$

In (44), $n_{W1}' \sim \mathcal{CN}(0, \sigma_W^2)$ and $n_{W2}' \sim \mathcal{CN}(0, \sigma_W^2)$ denote the AWGN at Willie 1 and Willie 2, respectively. As analyzed in Section III-B, the KL divergence is as the metric to evaluate the covertness. Given $\mathcal{H}0'$ and $\mathcal{H}1'$, the probability distributions of received signals at Willie 1/Willie 2 can be given as follows: $\mathbb{P}_0'^{W1} \triangleq f(y_{W1}'[m]|\mathcal{H}0) = \mathcal{CN}(0, \sigma_W^2)$, $\mathbb{P}_0'^{W2} \triangleq f(y_{W2}'[m]|\mathcal{H}0) = \mathcal{CN}(0, \sigma_W^2)$, $\mathbb{P}_1'^{W1} \triangleq f(y_{W1}'[m]|\mathcal{H}1) = \mathcal{CN}(0, |\sqrt{L_{RW}L_{RC}}\mathbf{g}_{RW}^H \boldsymbol{\Theta}_T' \mathbf{g}_{RC}|^2 P_C + |(\sqrt{L_{BW}} g_{BW} + \sqrt{L_{RW}L_{RB}}\mathbf{g}_{RW}^H \boldsymbol{\Theta}_R' \mathbf{g}_{RB}|^2 P_B + \sigma_W^2)$ and $\mathbb{P}_1'^{W2} \triangleq f(y_{W2}'[m]|\mathcal{H}1) = \mathcal{CN}(0, |\sqrt{L_{RL}L_{RB}}\mathbf{g}_{RL}^H \boldsymbol{\Theta}_T' \mathbf{g}_{RB}|^2 P_B + |(\sqrt{L_{CL}} g_{CL} + \sqrt{L_{RL}L_{RC}}\mathbf{g}_{RL}^H \boldsymbol{\Theta}_R' \mathbf{g}_{RC}|^2 P_C + \sigma_W^2)$. Therefore, the

KL divergences for Willie 1 and Willie 2 can be, respectively, calculated as

$$\mathcal{D}'_{W1} = \ln\left(1 + \frac{\sigma'^2_{\nu_1}}{\sigma^2_W}\right) + \frac{\sigma^2_W}{\sigma'^2_{\nu_1} + \sigma^2_W} - 1 \tag{45}$$

and

$$\mathcal{D}'_{W2} = \ln\left(1 + \frac{\sigma'^2_{\nu_2}}{\sigma^2_W}\right) + \frac{\sigma^2_W}{\sigma'^2_{\nu_2} + \sigma^2_W} - 1 \tag{46}$$

where $\sigma'^2_{\nu_1}$ and $\sigma'^2_{\nu_2}$ can be, respectively, given by

$$\sigma'^2_{\nu_1} = \left|\sqrt{L_{BW}} g_{BW} + \sqrt{L_{RW} L_{RB}} \mathbf{g}^H_{RW} \boldsymbol{\Theta}'_R \mathbf{g}_{RB}\right|^2 P_B + P_C \left|\sqrt{L_{RW} L_{RC}} \mathbf{g}^H_{RW} \boldsymbol{\Theta}'_T \mathbf{g}_{RC}\right|^2 \tag{47}$$

and

$$\sigma'^2_{\nu_2} = \left|\sqrt{L_{CL}} g_{CL} + \sqrt{L_{RL} L_{RC}} \mathbf{g}^H_{RL} \boldsymbol{\Theta}'_R \mathbf{g}_{RC}\right|^2 P_C + P_B \left|\sqrt{L_{RL} L_{RB}} \mathbf{g}^H_{RL} \boldsymbol{\Theta}'_T \mathbf{g}_{RB}\right|^2. \tag{48}$$

2) Expected Detection Performance: Having no access to the instantaneous CSI of the wardens, the expectation of the KL divergence is analyzed to evaluate the covertness of the networks. Here, we first analyze the probability distribution of $\sigma'^2_{\nu_1}$ and $\sigma'^2_{\nu_2}$.

Lemma 6: For a sufficiently large K, $\xi_{BW} = \mathbf{g}^H_{RW} \boldsymbol{\Theta}'_R \mathbf{g}_{RB}$, $\xi_{BL} = \mathbf{g}^H_{RL} \boldsymbol{\Theta}'_T \mathbf{g}_{RB}$, $\xi_{CL} = \mathbf{g}^H_{RL} \boldsymbol{\Theta}'_R \mathbf{g}_{RC}$ and $\xi_{CW} = \mathbf{g}^H_{RW} \boldsymbol{\Theta}'_T \mathbf{g}_{RC}$ can be approximated as four circularly symmetric complex Gaussian RVs with mean 0 and variance K, i.e.,

$$\xi_{BW}, \xi_{BL}, \xi_{CL}, \xi_{CW} \sim \mathcal{CN}(0, K). \tag{49}$$

Proof: Similar to the proof of Lemma 1. ∎

Based on Lemma 6, $\sigma'^2_{\nu_1}$ can be rewritten as

$$\sigma'^2_{\nu_1} = P_B(L_{BW} + KL_{RW}L_{RB})|\delta_0|^2 + P_C K L_{RW} L_{RC} |\delta_1|^2 \tag{50}$$

where $|\delta_0|^2, |\delta_1|^2 \sim \mathcal{CN}(0, 1)$. Denoting $\lambda_{BW} = P_B(L_{BW} + KL_{RW}L_{RB})$ and $\lambda_{CW} = P_C K L_{RW} L_{RC}$, the pdf of $\sigma'^2_{\nu_1}$ can be calculated as

$$f_{\sigma'^2_{\nu_1}}(x) = \frac{1}{\lambda_{CW} - \lambda_{BW}} \left(e^{-\frac{x}{\lambda_{CW}}} - e^{-\frac{x}{\lambda_{BW}}}\right). \tag{51}$$

Similarly, the pdf of $\sigma'^2_{\nu_2}$ can be calculated as

$$f_{\sigma'^2_{\nu_2}}(x) = \frac{1}{\lambda_{BL} - \lambda_{CL}} \left(e^{-\frac{x}{\lambda_{BL}}} - e^{-\frac{x}{\lambda_{CL}}}\right) \tag{52}$$

where $\lambda_{CL} = P_C(L_{CL} + KL_{RL}L_{RC})$ and $\lambda_{BL} = P_B K L_{RL} L_{RB}$. Therefore, the expectations of the KL divergences over all channels realizations are given in the following theorem.

Theorem 5: The expected values of $\mathcal{D}(\mathbb{P}'^{W1}_0 \| \mathbb{P}'^{W1}_1)$ over all realization of $\sigma'^2_{\nu_1}$ and $\mathcal{D}(\mathbb{P}'^{W2}_0 \| \mathbb{P}'^{W2}_1)$ over all realization of $\sigma'^2_{\nu_2}$ can be, respectively, given by

$$\mathcal{E}'_{W1} = \frac{\lambda_{BW} + \sigma^2_W}{\lambda_{CW} - \lambda_{BW}} \exp\left(\frac{\sigma^2_W}{\lambda_{BW}}\right) \mathrm{Ei}\left(-\frac{\sigma^2_W}{\lambda_{BW}}\right) - \frac{\lambda_{CW} + \sigma^2_W}{\lambda_{CW} - \lambda_{BW}} \exp\left(\frac{\sigma^2_W}{\lambda_{CW}}\right) \mathrm{Ei}\left(-\frac{\sigma^2_W}{\lambda_{CW}}\right) - 1 \tag{53}$$

and

$$\mathcal{E}'_{W2} = \frac{\lambda_{CL} + \sigma^2_W}{\lambda_{BL} - \lambda_{CL}} \exp\left(\frac{\sigma^2_W}{\lambda_{CL}}\right) \mathrm{Ei}\left(-\frac{\sigma^2_W}{\lambda_{CL}}\right) - \frac{\lambda_{BL} + \sigma^2_W}{\lambda_{BL} - \lambda_{CL}} \exp\left(\frac{\sigma^2_W}{\lambda_{BL}}\right) \mathrm{Ei}\left(-\frac{\sigma^2_W}{\lambda_{BL}}\right) - 1. \tag{54}$$

Proof: See Appendix F. ∎

In line with Theorem 5, the covertness of the STAR-RIS assisted uplink NOMA networks can be evaluated by means of the following constraints:

$$\mathcal{E}'_{W1} \le 2\varepsilon^2, \quad \text{and} \quad \mathcal{E}'_{W2} \le 2\varepsilon^2. \tag{55}$$

C. Covert STAR-RIS Uplink NOMA Design

Here, we first characterize the interruption performance of STAR-RIS assisted uplink NOMA networks. An optimization problem is then formulated to maximize the ECR of the uplink networks, subject to the constraints of covertness and reliability. Solving this problem, the optimal transmit powers at terminals are obtained.

1) Reliability Analysis: Due to the channel reciprocity, the cascaded channels between Alice and Bob/Cindy in the uplink NOMA networks are the same as those in the downlink NOMA networks. The probability distributions of cascaded channels are given in Lemmas 3 and 4. The cascaded channel from Bob to Alice is better than that from Cindy to Alice, hence Alice first decodes the signal of Cindy and then extracts the signal of Bob by employing the imperfect SIC. When the SINR decoding x_C or the SINR extracting x_B is below the preset value, the networks will be interrupted. The interruption probabilities of Alice are obtained as the following theorem.

Theorem 6: The interruption probabilities decoding x_C and x_B at Alice can be given by

$$\mathcal{P}_{A,C} = \sum_{n_1=1}^{N_a} \frac{\omega_{n_1} x_{n_1}^{k_B - 1}}{\Gamma(k_B)\Gamma(k_C)} \gamma\left(k_C, \frac{r_C P_B \theta_B x_{n_1} + r_C \sigma_0^2}{\theta_C P_C}\right) \tag{56}$$

and

$$\mathcal{P}_{A,B} = 1 - \left\{1 - \sum_{n_1=1}^{N_a} \gamma\left(k_C, \frac{r_C P_B \theta_B x_{n_1} + r_C \sigma_0^2}{\theta_C P_C}\right) \times \frac{\omega_{n_1} x_{n_1}^{k_B - 1}}{\Gamma(k_B)\Gamma(k_C)}\right\} \times \left\{1 - \sum_{n_1=1}^{N_a} \frac{\omega_{n_1} x_{n_1}^{k_C - 1}}{\Gamma(k_B)\Gamma(k_C)} \times \gamma\left(k_B, \frac{\varphi r_B P_C \theta_C x_{n_1} + r_B \sigma_0^2}{\theta_B P_B}\right)\right\} \tag{57}$$

respectively, where $\omega_i = [x_i/((n+1)^2 (L_{n+1}(x_i))^2)]$, $L_n(x) = [1/(n!)]([d/(dx)] - 1)^n x^n$ is the Laguerre polynomials [41], x_i is the ith root of $L_n(x)$ and N_a denotes the complexity-accuracy tradeoff parameter.

Proof: See Appendix G. ∎

2) Covert Transmission Principle: In the uplink NOMA network, Bob and Cindy attempt to covertly transmit the information to Alice aided by a STAR-RIS. The ECR for the uplink networks can be defined as $C^U_{\text{cov}} = (1 - \mathcal{P}_{A,B}) R_B + (1 - \mathcal{P}_{A,C}) R_C$. In order to improve the network performance, an ECR maximization problem is formulated by jointly optimizing the transmit power of the users, subject to the covertness

demands of the network, the reliability constraints of the users and maximum power constraint. The optimization problem can be described as follows:

$$\max_{P_B,P_C} \quad C_{\text{cov}}^{U} = \left(1-\mathcal{P}_{A,B}\right)R_B + \left(1-\mathcal{P}_{A,C}\right)R_C \tag{58a}$$

$$\text{s.t.} \quad \mathcal{E}'_{W1} \le 2\varepsilon^2 \tag{58b}$$

$$\mathcal{E}'_{W2} \le 2\varepsilon^2 \tag{58c}$$

$$\mathcal{P}_{A,B} \le p_B \tag{58d}$$

$$\mathcal{P}_{A,C} \le p_C \tag{58e}$$

$$0 < P_B + P_C \le p_{\max} \text{ and } P_B < P_C \tag{58f}$$

where $p_{\max}$ is the maximum scheduling power of uplink networks. The descriptions of other parameters are the same as those in Section IV-B. In the above, (58b) and (58c) are the covertness demands of the uplink network. Equations (58d) and (58e) are the reliability constraints of uplink users. Also, (58f) is the total power constraint of the network. Because of the complicated expressions of (53), (54), (56), and (57) and the coupled variables, it is difficult to find the closed-form solutions of this nonconvex problem. To tackle with address the issue, we transform (56) into a 2-D problem with specific bounds. Letting $P_B = \beta P_U$ and $P_C = (1-\beta)P_U$, (58f) can be equivalently converted to $0 < P_U \le p_{\max}$ and $0 < \beta < 0.5$. P_U can be regarded as the total power of the uplink network. Therefore, (58) can be reduced to

$$\max_{P_U,\beta} \quad C_{\text{cov}}^{U} = \left(1-\mathcal{P}_{A,B}\right)R_B + \left(1-\mathcal{P}_{A,C}\right)R_C \tag{59a}$$

$$\text{s.t.} \quad 0 < P_U \le p_{\max} \text{ and } 0 < \beta < 0.5 \tag{59b}$$

$$(58\text{b})-(58\text{e}).$$

The above problem can be solved by a 2-D numerical search over the intervals $(0, 0.5)$ and $(0, p_{\max}]$. It is noted that the 2-D numerical search is efficient since the lower and upper bounds β and P_U are explicitly given. Substituting the optimal β^* and P_U^* into $P_B = \beta P_U$ and $P_C = (1-\beta)P_U$, the optimal P_B^* and P_C^* are gotten. Consequently, the maximum ECR of the uplink network is obtained.

V. Numerical Results and Discussion

In this section, numerical results are provided to validate the proposed scheme for the downlink and uplink NOMA networks. For evaluating the superiority of the proposed scheme, this article considers three benchmarks: STAR-RIS assisted OMA scheme, the relay assisted NOMA scheme and the relay assisted OMA scheme.

Unless otherwise specified, the system parameters for the networks are set as follows: $m_\Delta = 2$, $\beta = 3$, $\phi = 0.1$, $\sigma_w^2 = \sigma_0^2 = 0.1$ W, $r_c = 0.4$ bps/Hz, $r_b = 0.6$ bps/Hz, $p_B = p_C = 0.1$, $d_{ab} = d_{rc} = 5$ and $d_{ar} = d_{aw} = d_{rw} = d_{rb} = d_{rl} = d_{cl} = 10$ m.

A. STAR-RIS Downlink NOMA Networks

Fig. 3 shows the relationships between $\mathcal{E}_{W1}$ and $\mathcal{E}_{W2}$ and P_A for different values of K in the downlink NOMA networks, where EKLD denotes the expected values of KL divergence for the downlink networks: $\mathcal{E}_{W1}$ or $\mathcal{E}_{W2}$. It can be observed from Fig. 3 that both $\mathcal{E}_{W1}$ and $\mathcal{E}_{W2}$ are proportional to P_A. By increasing the transmit power, Willie 1 and Willie 2 are more likely to detect the information transmissions. This results in reduced detection error probabilities at Willie 1 and Willie 2 and thus increases $\mathcal{E}_{W1}$ and $\mathcal{E}_{W2}$. In practice, the transmit power should be reasonably controlled in the light of the covertness demand such that the wardens cannot effectively detect the communication behaviors of the networks. Also, Fig. 3 indicates that both $\mathcal{E}_{W1}$ and $\mathcal{E}_{W2}$ are proportional to K. This is because the larger the K, the better the channels quality of Willie 1 and Willie 2, and the more likely Willie 1 and Willie 2 are to detect the communication behaviors. Additionally, as it is seen, the simulation results verify the accuracy of the theoretical results.

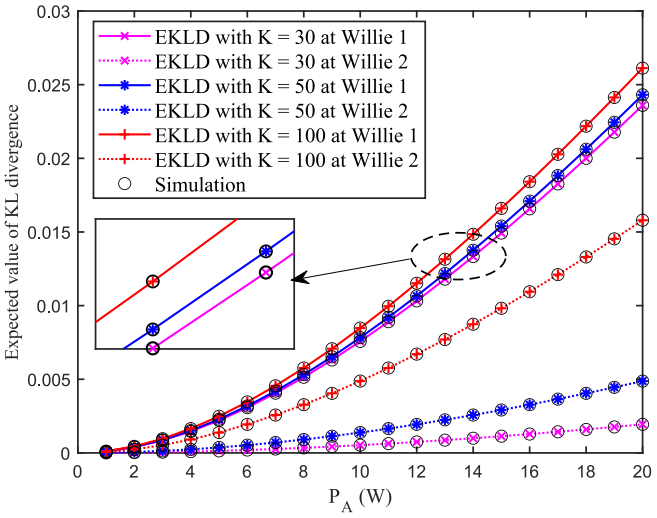

Fig. 3. $\mathcal{E}_{W1}$ and $\mathcal{E}_{W2}$ versus P_A for different values of K in the STAR-RIS downlink NOMA networks.

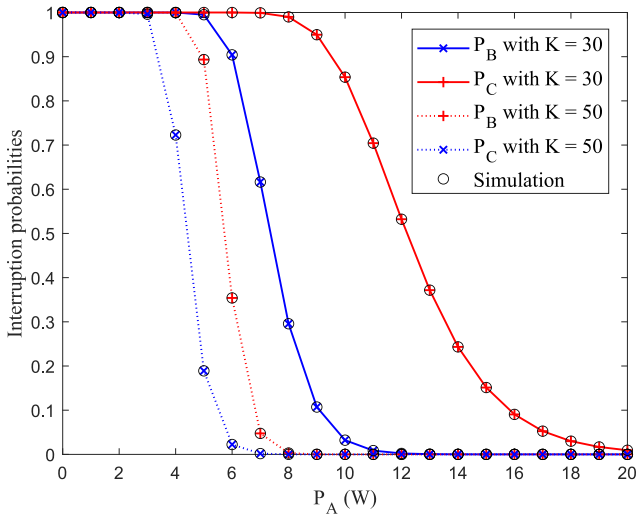

Fig. 4. $\mathcal{P}_B$ and $\mathcal{P}_C$ versus P_A for different values of K in the STAR-RIS downlink NOMA network.

Figs. 4 and 5 demonstrate the relationships between the interruption probabilities and P_A with a_1, respectively. It is seen that both $\mathcal{P}_B$ and $\mathcal{P}_C$ are inversely proportional to P_A. By increasing P_A, the power of signals received at Bob and Cindy increases. As such, the users become more capable to

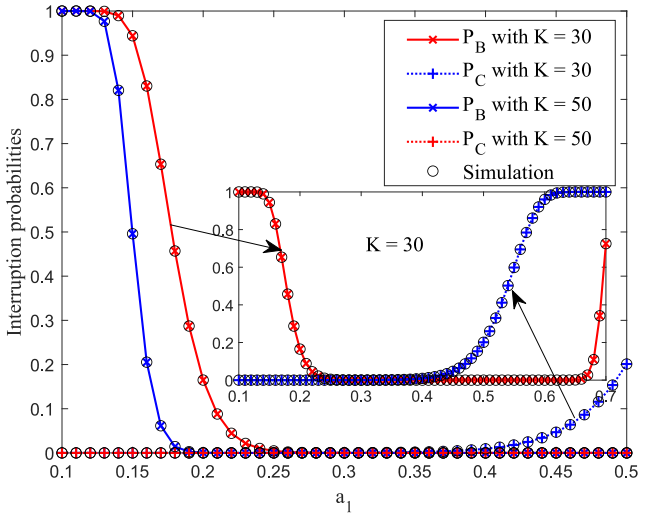

Fig. 5. $\mathcal{P}_B$ and $\mathcal{P}_C$ versus a_1 for different values of K in the STAR-RIS downlink NOMA network.

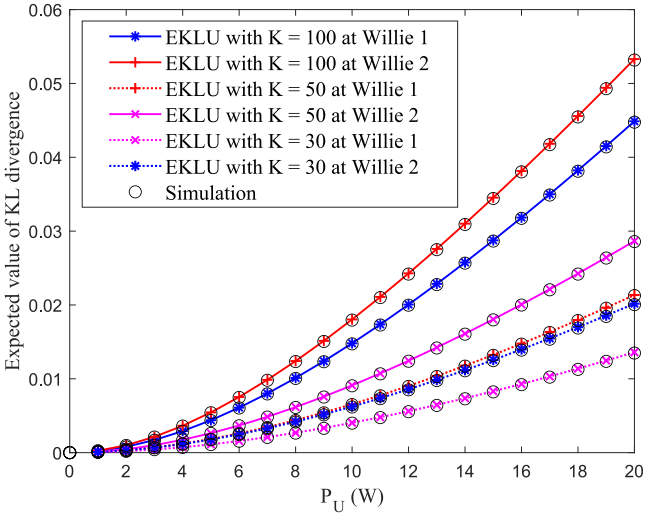

Fig. 7. $\mathcal{E}'_{W1}$ and $\mathcal{E}'_{W2}$ versus P_U for different values of K in the STAR-RIS uplink NOMA networks.

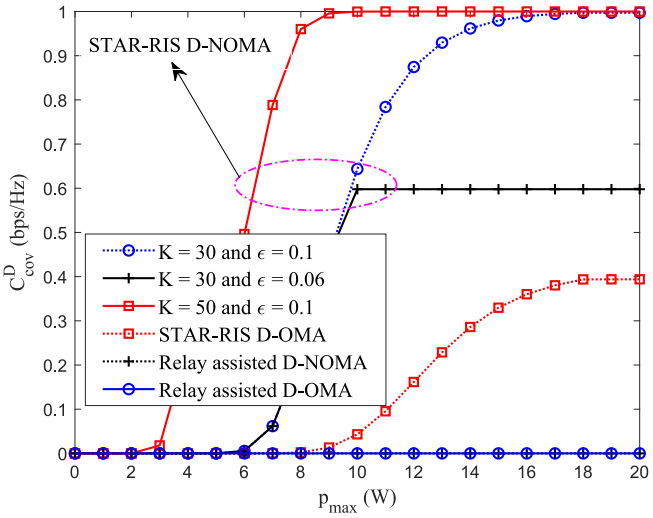

Fig. 6. C^D_{cov} for the different schemes in the downlink networks.

decode the signals, which makes $\mathcal{P}_B$ and $\mathcal{P}_C$ lower. For Bob and Cindy, in order to ensure the reliable transmission, P_A should be set as large as possible under the constraints of the networks. Fig. 5 also shows that $\mathcal{P}_B$ first decreases and then increases and $\mathcal{P}_C$ increases with an increase of a_1. As a_1 increases, more power is allocated to x_B and less power is allocated to x_C. As a result, it gets harder for Cindy to decode x_C and thus $\mathcal{P}_C$ gets larger. For Bob, he needs to first decoded x_C and then x_B. By increasing a_1, decoding x_B becomes easier. When a_1 increases to a specific value (e.g., $a_1 = 0.66$ as in Fig. 5), Bob decodes x_C with a decoding error, causing $\mathcal{P}_B$ to decrease first and then increase. In practice, a_1 should be set within $(0, 0.5)$ due to the fairness and the reliability. Figs. 4 and 5 also indicate that $\mathcal{P}_B$ and $\mathcal{P}_C$ are inversely proportional to K, which demonstrates that the STAR-RIS can enhance the reliability of the networks. Also, simulations in Figs. 4 and 5 verify the analysis in this article.

Fig. 6 compares the ECR of the proposed scheme and three benchmarks for the downlink scenario. In the figure, D-OMA and D-NOMA, respectively, means the downlink OMA and NOMA. As it is seen, the proposed STAR-RIS assisted D-NOMA scheme outperforms three benchmarks in terms of the ECR C^D_{cov}. This is because, for the STAR-RIS assisted D-OMA scheme, its covertness is the same as the proposed scheme, but its interruption performance is lower than the proposed scheme with the NOMA. For the relay assisted D-NOMA and D-OMA scheme, the power of multiple observations at the wardens is the same without the phase or power uncertainty. Once Alice sends the signals, wardens can detect the existence of the communications, so the ECRs are equal to 0. Fig. 6 also shows the trend of C^D_{cov} w.r.t. the maximum transmit power $p_{\max}$ for the different covertness demands ε. It is observed that C^D_{cov} reaches its maximum value and levels off when $p_{\max}$ grows to a certain value. In addition, for smaller ε, C^D_{cov} cannot reach its maximum. This is because when the covertness demand is higher, Alice cannot send signals with the high power, otherwise the transmissions might be detected by wardens. Further, Fig. 6 shows the increasing the number of the elements of STAR-RIS can enhance C^D_{cov} of the downlink NOMA networks under the same covertness constraint.

B. STAR-RIS Uplink NOMA Networks

It is worth noting that the decoding SINR is different for the uplink and downlink scenario, according to (3)–(5) and (42) and (43). For the downlink scenario, the channel coefficients on the numerator and denominator of the SINR in (3)–(5) are from the same user and the same. However, for the uplink scenario, Alice simultaneously receives the signals from Bob and Cindy, so the channel coefficients on the numerator and denominator of the SINR are different in (42) and (43). If they differ too much, for example, if a direct link exists for one user and not for another, there may be an order of magnitude difference in the power allocated to each uplink user. Therefore, for the sake of user fairness, it is considered that neither user has a direct link and some parameters are adjusted as follows: $d_{rb} = 4$ m and $d_{rc} = 4.5$ m.

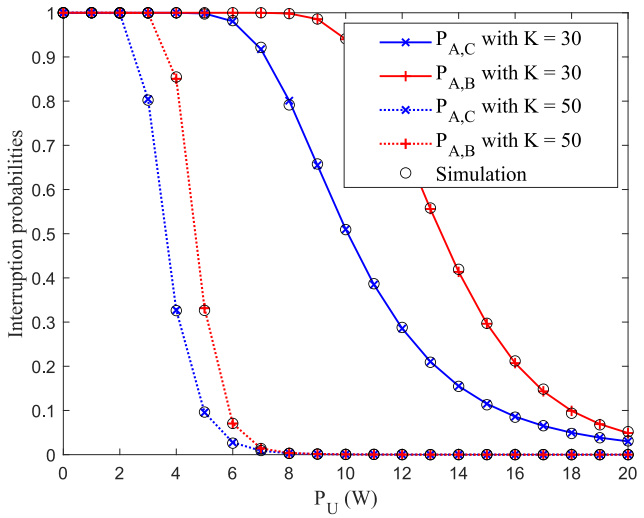

Fig. 8. $\mathcal{P}_{A,B}$ and $\mathcal{P}_{A,C}$ versus P_U for different values of K in the STAR-RIS uplink NOMA network.

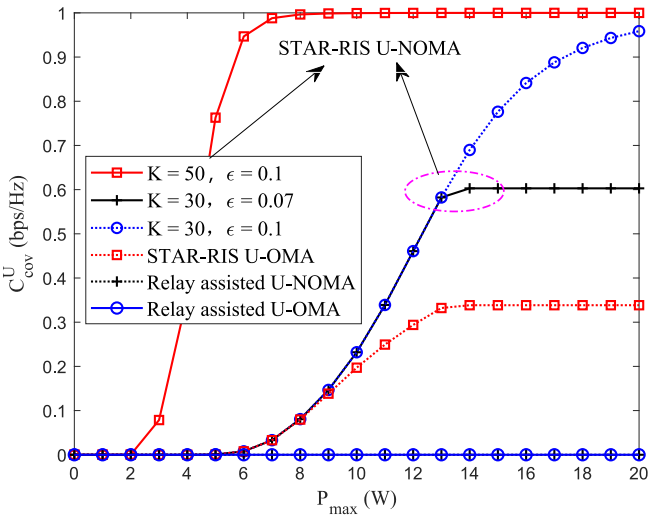

Fig. 9. C_{cov}^{U} for the different schemes in the uplink networks.

Fig. 7 depicts the relationships between $\mathcal{E}'_{W1}$ and $\mathcal{E}'_{W2}$ and the total power P_U of the uplink networks. It is observed that both $\mathcal{E}'_{W1}$ and $\mathcal{E}'_{W2}$ increase with P_U. The reason is that the larger the total power in the uplink networks, the more signals exposed to Willie 1 and Willie 2 and the higher the probability of successful detection by Willie 1 and Willie 2. To ensure the covertness of the transmissions, P_U should be carefully selected. Fig. 7 also depicts the effect of K on $\mathcal{E}'_{W1}$ and $\mathcal{E}'_{W2}$ for the uplink networks. It is seen that $\mathcal{E}'_{W1}$ and $\mathcal{E}'_{W2}$ increase with K. This is because the larger the K, the better the channels condition of Willie 1 and Willie 2, and the more likely Willie 1 and Willie 2 are to detect the transmission behaviors. Furthermore, simulations in Fig. 7 also verify the accuracy of the analysis.

Fig. 8 demonstrates the relationships between the interruption probabilities, $\mathcal{P}_{A,B}$ and $\mathcal{P}_{A,C}$, and the total power P_U for the STAR-RIS assisted uplink NOMA networks. It can be seen that both $\mathcal{P}_{A,B}$ and $\mathcal{P}_{A,C}$ reduces with the increase of P_U. This is because the larger the P_U, the more power allocated to the signals of Bob and Cindy and the easier it is for Alice to decode x_B and x_C. As a result, both $\mathcal{P}_{A,B}$ and $\mathcal{P}_{A,C}$ are subsequently lowered. In practice, the reliability and covertness of the networks should be guaranteed at the same time. To this end, this article formulates a resource allocation strategy to balance the reliability and covertness for the uplink networks in (58). Additionally, it is also observed that increasing K can improve the interruption performance of the uplink networks by enhancing the cascaded channel gain. Further, simulation results verify the accuracy of the analytical results.

Fig. 9 compares the ECR C_{cov}^{U} of the proposed scheme and three benchmarks for the uplink scenario. In the figure, U-OMA and U-NOMA, respectively, denotes the uplink OMA and NOMA. It is seen in Fig. 9 that the ECR of the proposed scheme is greater than that of three benchmarks. The reasons are as follows. For the STAR-RIS assisted U-OMA scheme, the decoding SINR of Alice is below that for the NOMA protocol. For relay assisted U-OMA and U-NOMA schemes, multiple observations are the same without phase or power uncertainty. Once transmitted, the wardens can detect the communication successfully. For the proposed scheme, the SIC decreases the interference between users and improves the decoding SINR of Alice. At the same time, the phase shifting of the STAR-RIS confuses the wardens. Therefore, the ECR is boosted. In addition, Fig. 9 also indicates that ECR C_{cov}^{U} first increases and then stabilizes to a maximum value, with the increase of the maximum scheduling power $p_{\max}$ of uplink networks. For the different covertness demand, i.e., the different value of ε, the achievable maximum C_{cov}^{U} is different. The higher the covertness demand, the lower the power that can be utilized to transmit, and the lower the achievable maximum C_{cov}^{U}. Conversely, the lower the covertness demand, the larger the achievable maximum C_{cov}^{U}. Furthermore, Fig. 9 shows the increasing the number of the elements of the STAR-RIS can enhance C_{cov}^{U} of the uplink networks under the same covertness constraint.

VI. Conclusion

This article considered the covert communication in STAR-RIS assisted NOMA networks over Nakagami-m fading channels for downlink and uplink IoT scenarios. Under the NOMA protocol with the imperfect SIC, an IoT access point attempted to achieve information interaction with two IoT users aided by a STAR-RIS. The two IoT users were located at both sides of the STAR-RIS, where Bob was the near user and Cindy was the far user. Bob and Cindy were monitored by Willie 1 and Willie 2, respectively. The phase shifting of STAR-RIS provided users with a shelter for covert transmissions. In this article, KL divergence was used to evaluate the detection performance of wardens. The cascaded channels gains of users and wardens were, respectively, approximated as Gamma and complex Gaussian RVs. Without the instantaneous CSI of wardens, the expectations of KL divergence were characterized. In order to measure the reliability, the interruption probabilities of the networks were derived. For the downlink scenario, by jointly optimizing the transmit power and power allocation coefficient of the IoT access

point, the ECR of the downlink networks was maximized. For the uplink scenario, by jointly the transmit power of users, the ECR of the uplink networks was maximized. The two maximization problems were, respectively, solved analytically, subject to the covertness demands, reliability constraints and power boundary constraints. Simulation results showed that applying STAR-RIS into NOMA IoT networks could bring more covertness gain as compared with benchmarks. In the future, considering the delay requirements of emerging IoT applications, we would focus on the covert transmission with the finite blocklength in the STAR-RIS assisted NOMA IoT network.

Appendix A
Proof of Lemma 3

According to (31), ξ_B can be rewritten as

$$\xi_B = \sqrt{L_{AB}}|g_{AB}| + \sqrt{L_{AR}L_{RB}}\sum_{k=1}^{K}|g_{AR}||g_{RB}| = \sum_{k=1}^{K}\left(\sqrt{\frac{L_{AB}}{K^2}}|g_{AB}| + \sqrt{L_{AR}L_{RB}}|g_{AR}||g_{RB}|\right). \quad (60)$$

Define $h_{AB} = \sqrt{(L_{AB}/K^2)}|g_{AB}| + \sqrt{L_{AR}L_{RB}}|g_{AR}||g_{RB}|$. We can calculate the expectation and variance of h_{AB}, respectively, as

$$\mathbb{E}(h_{AB}) = \sqrt{\frac{L_{AB}\pi}{2K^2}} + \sqrt{L_{AR}L_{RB}}\Omega_{m_{AB}} \quad (61)$$

and

$$\mathbb{V}(h_{AB}) = \frac{L_{AB}(4-\pi)}{2K^2} + L_{AR}L_{RB}\left(1-\Omega_{m_{AB}}^2\right). \quad (62)$$

In line with the CLT, ξ_B can be approximated as a Gaussian RV distributed on $\mathcal{N}(K\mathbb{E}(h_{AB}), K\mathbb{V}(h_{AB}))$. By means of [22, Corollary 1], Lemma 3 can be proved.

Appendix B
Proof of Lemma 4

Define $h_{AC} = \sqrt{L_{AR}L_{RC}}|g_{AR}||g_{RC}|$. The expectation and variance of h_{AC} can be, respectively, calculated as

$$\mathbb{E}(h_{AC}) = \sqrt{L_{AR}L_{RC}}\Omega_{m_{AC}} \quad (63)$$

and

$$\mathbb{V}(h_{AC}) = L_{AR}L_{RC}\left(1-\Omega_{m_{AC}}^2\right). \quad (64)$$

In line with the CLT, ξ_C can be approximated as a Gaussian RV distributed on $\mathcal{N}(K\mathbb{E}(h_{AC}), K\mathbb{V}(h_{AC}))$. By means of [22, Corollary 1]], Lemma 4 can be proved.

Appendix C
Proof of Theorem 3

It is assumed that Bob has a better channel condition, so Bob first decodes x_C and then extracts x_B by removing x_C. Considering the imperfect SIC, the interruption probability at Bob can be calculated by

$$\mathcal{P}_B = 1 - \mathbb{P}\left(\gamma_{B,C} > r_C\right)\mathbb{P}(\gamma_B > r_B) \quad (65)$$

where

$$\mathbb{P}\left(\gamma_{B,C} > r_C\right) = \mathbb{P}\left(\frac{|\xi_B|^2 a_2 P_A}{|\xi_B|^2 a_1 P_A + \sigma_0^2} > r_C\right) = \mathbb{P}\left(|\xi_B|^2 > \frac{\sigma_0^2 r_C}{(a_2 - a_1 r_C)P_A}\right) \overset{(d)}{=} 1 - \frac{1}{\Gamma(k_B)}\gamma\left(k_B, \frac{\sigma_0^2 r_C}{\theta_B(a_2 - a_1 r_C)P_A}\right) \quad (66)$$

and

$$\mathbb{P}(\gamma_B > r_B) = \mathbb{P}\left(\frac{|\xi_B|^2 a_1 P_A}{\phi|\xi_B|^2 a_2 P_A + \sigma_0^2} > r_B\right) = \mathbb{P}\left(|\xi_B|^2 > \frac{\sigma_0^2 r_B}{(a_1 - \phi a_2 r_B)P_A}\right) \overset{(d)}{=} 1 - \frac{1}{\Gamma(k_B)}\gamma\left(k_B, \frac{\sigma_0^2 r_B}{\theta_B(a_1 - \phi a_2 r_B)P_A}\right) \quad (67)$$

where (d) follows by utilizing the distribution probability of $|\xi_B|^2$ in the integral. Substituting (66) and (67) into (65), the closed-form expression of $\mathcal{P}_B$ is obtained and Theorem 3 is proved.

Appendix D
Proof of Theorem 4

As a far user, Cindy decodes x_C by regarding x_B as the interference. Based on Lemma 4, the interruption probability at Cindy can be calculated by

$$\mathcal{P}_C = \mathbb{P}(\gamma_C < r_C) = \mathbb{P}\left(\frac{|\xi_C|^2 a_2 P_A}{|\xi_C|^2 a_1 P_A + \sigma_0^2} < r_C\right) = \mathbb{P}\left(|\xi_C|^2 < \frac{\sigma_0^2 r_C}{(a_2 - a_1 r_C)P_A}\right) = \frac{1}{\Gamma(k_C)}\gamma\left(k_C, \frac{\sigma_0^2 r_C}{\theta_C(a_2 - a_1 r_C)P_A}\right). \quad (68)$$

This completes the proof.

Appendix E
Proof of Lemma 5

Define $b(x) = -(1+x)\exp(x)\mathrm{Ei}(-x)$, for $x > 0$. The first-order derivative of $b(x)$ w.r.t. x can be calculated by

$$\frac{db(x)}{dx} = -\left((x+2)\exp(x)\mathrm{Ei}(-x) + \frac{x+1}{x}\right) = (x+2)e^x\left(\int_x^{\infty}\frac{\exp(-t)}{t}dt - \frac{x+1}{x(x+2)\exp(x)}\right). \quad (69)$$

Define $c(x) = (x+1)/(x(x+2)\exp(x))$, and its first-order derivative w.r.t. x can be calculated as

$$\frac{dc(x)}{dx} = \frac{\exp(-x)\left(-2 - x(x+2)^2\right)}{x^2(x+2)^2}. \quad (70)$$

Note that $[(dc(x))/(dx)]$ is continuous for $x > 0$. Thus

$$\int_x^{\infty}\frac{e^{-t}\left(-2 - t(t+2)^2\right)}{t^2(t+2)^2}dt = c(\infty) - c(x) = -c(x). \quad (71)$$

Substituting (71) into (69), $[(db(x))/(dx)]$ can be rewritten as

$$\frac{db(x)}{dx} = (x+2)e^x \int_x^\infty \frac{-2\exp(-t)}{t^2(t+2)^2}dt \tag{72}$$

which is always less than or equal to 0, for $x > 0$. Therefore, $b(x)$ is a monotonically decreasing function w.r.t. x. $\mathcal{E}_{W1} = b(\sigma_W^2/\lambda_{W1}) = b[(\sigma_W^2)/(P_A(L_{AW} + KL_{AR}L_{RW}))]$ is a monotonically increasing function w.r.t. P_A. Similarly, $\mathcal{E}_{W2}$ is also a monotonically increasing function w.r.t. P_A. This completes the proof.

Appendix F
Proof of Theorem 5

According to (45), the expected value of $\mathcal{D}(\mathbb{P}_0'^{W1}\|\mathbb{P}_1'^{W1})$ over all realization of $\sigma_{\nu_1}'^2$ can be calculated as

$$\begin{aligned}\mathcal{E}'_{W1} &= \int_0^\infty \left(\ln\left(1+\frac{x}{\sigma_W^2}\right) + \frac{\sigma_W^2}{x+\sigma_W^2}\right) f_{\sigma_{\nu_1}'^2}(x)dx - 1 \\ &= \int_0^\infty \left(\ln\left(1+\frac{x}{\sigma_W^2}\right) + \frac{\sigma_W^2}{x+\sigma_W^2}\right) \frac{1}{\lambda_{CW}-\lambda_{BW}} \\ &\quad \times \left(e^{-\frac{x}{\lambda_{CW}}} - e^{-\frac{x}{\lambda_{BW}}}\right)dx - 1 \\ &\overset{(e)}{=} \frac{\lambda_{BW}+\sigma_W^2}{\lambda_{CW}-\lambda_{BW}} \exp\left(\frac{\sigma_W^2}{\lambda_{BW}}\right) \mathrm{Ei}\left(-\frac{\sigma_W^2}{\lambda_{BW}}\right) \\ &\quad - \frac{\lambda_{CW}+\sigma_W^2}{\lambda_{CW}-\lambda_{BW}} \exp\left(\frac{\sigma_W^2}{\lambda_{CW}}\right) \mathrm{Ei}\left(-\frac{\sigma_W^2}{\lambda_{CW}}\right) - 1 \end{aligned} \tag{73}$$

where the step (e) can refer to the computational procedure of Theorem 1. Also, the derivation of $\mathcal{E}'_{W2}$ is the same as that of $\mathcal{E}'_{W1}$. As such, the proof is complete.

Appendix G
Proof of Theorem 6

At Alice, x_C is first decoded. Based on (42), the interruption probability decoding x_C at Alice can be calculated by

$$\begin{aligned}\mathcal{P}_{A,C} &= \mathbb{P}(\gamma_{A,C} < r_C) = \mathbb{P}\left(\frac{|\xi_C|^2 P_C}{|\xi_B|^2 P_B + \sigma_0^2} < r_C\right) \\ &= \int_0^\infty \int_0^{\frac{r_C P_B}{P_C}y + \frac{r_C\sigma_0^2}{P_C}} f_{|\xi_C|^2}(x) f_{|\xi_B|^2}(y)dxdy \\ &= \int_0^\infty \frac{1}{\Gamma(k_C)}\gamma\left(k_C, \frac{r_C P_B x + r_C\sigma_0^2}{P_C}\right) \frac{x^{k_B-1}e^{-\frac{x}{\theta_B}}}{\Gamma(k_B)\theta_B^{k_B}}dx \\ &\overset{(f)}{=} \sum_{n_1=1}^{N_a} \frac{\omega_{n_1} x_{n_1}^{k_B-1}}{\Gamma(k_B)\Gamma(k_C)} \gamma\left(k_C, \frac{r_C P_B \theta_B x_{n_1} + r_C\sigma_0^2}{P_C}\right) \end{aligned} \tag{74}$$

where the Gauss-Laguerre quadrature [41, eq. (25.4.45)] is used in (f). For the imperfect SIC, the interruption probability decoding x_B at Alice is therefore

$$\begin{aligned}\mathcal{P}_{A,B} &= 1 - \mathbb{P}(\gamma_{A,C} > r_C)\mathbb{P}(\gamma_{A,B} > r_B) \\ &= 1 - \big(1 - \mathbb{P}(\gamma_{A,C} < r_C)\big)\big(1 - \mathbb{P}(\gamma_{A,B} < r_B)\big) \end{aligned} \tag{75}$$

where $\mathbb{P}(\gamma_{A,B} < r_B)$ can be calculated similar to (74). Straightforward algebraic manipulations proves Theorem 6.

References

[1] D. Zhou, M. Sheng, J. Li, and Z. Han, "Aerospace integrated networks innovation for empowering 6G: A survey and future challenges," *IEEE Commun. Surveys Tuts.*, vol. 25, no. 2, pp. 975–1019, 2nd Quart., 2023,

[2] D. C. Nguyen et al., "6G Internet of Things: A comprehensive survey," *IEEE Internet Things J.*, vol. 9, no. 1, pp. 359–383, Jan. 2022.

[3] F. Guo, F. R. Yu, H. Zhang, X. Li, H. Ji, and V. C. M. Leung, "Enabling massive IoT toward 6G: A comprehensive survey," *IEEE Internet Things J.*, vol. 8, no. 15, pp. 11891–11915, Aug. 2021.

[4] N.-N. Dao et al., "Survey on aerial radio access networks: Toward a comprehensive 6G access infrastructure," *IEEE Commun. Surveys Tuts.*, vol. 23, no. 2, pp. 1193–1225, 2nd Quart., 2021.

[5] Z. Ding et al., "A state-of-the-art survey on reconfigurable intelligent surface-assisted non-orthogonal multiple access networks," *Proc. IEEE*, vol. 110, no. 9, pp. 1358–1379, Sep. 2022

[6] O. Maraqa et al., "A survey of rate-optimal power domain NOMA with enabling technologies of future wireless networks," *IEEE Commun. Surveys Tuts.*, vol. 22, no. 4, pp. 2192–2235, 4th Quart., 2020.

[7] Y. Bai, W. Chen, B. Ai, Z. Zhong, and I. J. Wassell, "Prior information aided deep learning method for grant-free NOMA in mMTC," *IEEE J. Sel. Areas Commun.*, vol. 40, no. 1, pp. 112–126, Jan. 2022.

[8] X. Mu et al., "Intelligent reflecting surface enhanced multi-UAV NOMA networks," *IEEE J. Sel. Areas Commun.*, vol. 39, no. 10, pp. 3051–3066, Oct. 2021.

[9] Y. Liu, Y. Deng, M. Elkashlan, A. Nallanathan, and G. K. Karagiannidis, "Optimization of grant-free NOMA with multiple configured-grants for mURLLC," *IEEE J. Sel. Areas Commun.*, vol. 40, no. 4, pp. 1222–1236, Apr. 2022.

[10] Y. Liu et al., "Reconfigurable intelligent surfaces: Principles and opportunities," *IEEE Commun. Surveys Tuts.*, vol. 23, no. 3, pp. 1546–1577, 3rd Quart., 2021.

[11] C. Huang et al., "Reconfigurable intelligent surfaces for energy efficiency in wireless communication," *IEEE Trans. Wireless Commun.*, vol. 18, no. 8, pp. 4157–4170, Aug. 2019.

[12] G. Chen, Q. Wu, C. He, W. Chen, J. Tang, and S. Jin, "Active IRS aided multiple access for energy-constrained IoT systems," *IEEE Trans. Wireless Commun.*, vol. 22, no. 3, pp. 1677–1694, Mar. 2023.

[13] Z. Chu, P. Xiao, D. Mi, W. Hao, Q. Chen, and Y. Xiao, "IRS-assisted wireless powered IoT network with multiple resource blocks," *IEEE Trans. Commun.*, vol. 71, no. 4, pp. 2335–2350, Apr. 2023.

[14] S. Li et al., "IRS-assisted full duplex systems over Rician and Nakagami fading channels," *IEEE Open J. Veh. Technol.*, vol. 4, pp. 217–229, Jan. 2023.

[15] B. Tahir, S. Schwarz, and M. Rupp, "Analysis of uplink IRS-assisted NOMA under Nakagami-m fading via moments matching," *IEEE Wireless Commun. Lett.*, vol. 10, no. 3, pp. 624–628, Mar. 2021.

[16] Z. Ding, R. Schober, and H. V. Poor, "On the impact of phase shifting designs on IRS-NOMA," *IEEE Wireless Commun. Lett.*, vol. 9, no. 10, pp. 1596–1600, Oct. 2020.

[17] T. Wang, F. Fang, and Z. Ding, "An SCA and relaxation based energy efficiency optimization for multi-user RIS-assisted NOMA networks," *IEEE Trans. Veh. Technol.*, vol. 71, no. 6, pp. 6843–6847, Jun. 2022.

[18] Y. Zou, Y. Liu, X. Mu, X. Zhang, Y. Liu, and C. Yuen, "Machine learning in RIS-assisted NOMA IoT networks," *IEEE Internet Things J.*, vol. 10, no. 22, pp. 19427–19440, Nov. 2023.

[19] H. Zhang and B. Di, "Intelligent omni-surfaces: Simultaneous refraction and reflection for full-dimensional wireless communications," *IEEE Commun. Surveys Tuts.*, vol. 24, no. 4, pp. 1997–2028, 4th Quart., 2022.

[20] C. Wu, Y. Liu, X. Mu, X. Gu, and O. A. Dobre, "Coverage characterization of STAR-RIS networks: NOMA and OMA," *IEEE Commun. Lett.*, vol. 25, no. 9, pp. 3036–3040, Sep. 2021.

[21] W. Du et al., "STAR-RIS assisted wireless powered IoT networks," *IEEE Trans. Veh. Technol.*, vol. 72, no. 8, pp. 10644–10658, Aug. 2023.

[22] Z. Xie, W. Yi, X. Wu, Y. Liu, and A. Nallanathan, "STAR-RIS aided NOMA in multicell networks: A general analytical framework with gamma distributed channel modeling," *IEEE Trans. Commun.*, vol. 70, no. 8, pp. 5629–5644, Aug. 2022.

[23] T. Wang, M.-A. Badiu, G. Chen, and J. P. Coon, "Outage probability analysis of STAR-RIS assisted NOMA network with correlated channels," *IEEE Commun. Lett.*, vol. 26, no. 8, pp. 1774–1778, Aug. 2022.

[24] H. Liu et al., "Effective capacity analysis of STAR-RIS-assisted NOMA networks," *IEEE Wireless Commun. Lett.*, vol. 11, no. 9, pp. 1930–1934, Sep. 2022.

[25] X. Li, Y. Zheng, M. Zeng, Y. Liu, and O. A. Dobre "Enhancing secrecy performance for STAR-RIS NOMA networks," *IEEE Trans. Veh. Technol.*, vol. 72, no. 2, pp. 2684–2688, Feb. 2023.
[26] F. Fang, B. Wu, S. Fu, Z. Ding, and X. Wang, "Energy-efficient design of STAR-RIS aided MIMO-NOMA networks," *IEEE Trans. Commun.*, vol. 71, no. 1, pp. 498–511, Jan. 2023.
[27] Y. Su, X. Pang, W. Lu, N. Zhao, X. Wang, and A. Nallanathan, "Joint location and beamforming optimization for STAR-RIS aided NOMA-UAV networks," *IEEE Trans. Veh. Technol.*, vol. 72, no. 8, pp. 11023–11028, Aug. 2023.
[28] C. Gao, B. Yang, X. Jiang, H. Inamura, and M. Fukush "Covert communication in relay-assisted IoT systems," *IEEE Internet Things J.*, vol. 8, no. 8, pp. 6313–6323, Apr. 2021.
[29] M. Wang, W. Yang, X. Lu, C. Hu, B. Liu, and X. Lv, "Channel inversion power control aided covert communications in uplink NOMA systems," *IEEE Wireless Commun. Lett.*, vol. 11, no. 4, pp. 871–875, Apr. 2022.
[30] L. Tao, W. Yang, S. Yan, D. Wu, X. Guan, and D. Chen, "Covert communication in downlink NOMA systems with random transmit power," *IEEE Wireless Commun. Lett.*, vol. 9, no. 11, pp. 2000–2004, Nov. 2020.
[31] Z. Duan, X. Yang, Y. Gong, D. Wang, and L. Wang, "Covert communication in uplink NOMA systems under channel distribution information uncertainty," *IEEE Commun. Lett.*, vol. 27, no. 5, pp. 1282–1286, May 2023.
[32] L. Tao, W. Yang, X. Lu, M. Wang, and Y. Song "Achieving covert communication in uplink NOMA systems via energy harvesting jammer," *IEEE Commun. Lett.*, vol. 25, no. 12, pp. 3785–3789, Dec. 2021.
[33] P. Liu, Z. Li, J. Si, N. Al-Dhahir, and Y. Gao, "Joint information-theoretic secrecy and covertness for UAV-assisted wireless transmission with finite blocklength," *IEEE Trans. Veh. Technol.*, vol. 72, no. 8, pp. 10187–10199, Aug. 2023.
[34] S. Ma et al., "Covert beamforming design for intelligent-reflecting-surface-assisted IoT networks," *IEEE Internet Things J.*, vol. 9, no. 7, pp. 5489–5501, Apr. 2022.
[35] M. T. Mamaghani and Y. Hong, "Aerial intelligent reflecting surface-enabled terahertz covert communications in beyond-5G Internet of Things," *IEEE Internet Things J.*, vol. 9, no. 19, pp. 19012–19033, Oct. 2022.
[36] C. Wang et al., "Intelligent reflecting surface-aided full-duplex covert communications: Information freshness optimization," *IEEE Trans. Wireless Commun.*, vol. 22, no. 5, pp. 3246–3263, May 2023.
[37] C. Chen, M. Wang, B. Xia, Y. Guo, and J. Wang, "Performance analysis and optimization of IRS-aided covert communication with hardware impairments," *IEEE Trans. Veh. Technol.*, vol. 72, no. 4, pp. 5463–5467, Apr. 2023.
[38] L. Lv, Q. Wu, Z. Li, Z. Ding, N. Al-Dhahir, and J. Chen, "Covert communication in intelligent reflecting surface-assisted noma systems: Design, analysis, and optimization," *IEEE Trans. Wireless Commun.*, vol. 21, no. 3, pp. 1735–1750, Mar. 2022.
[39] L. Yang et al., "Covert transmission and secrecy analysis of RS-RIS-NOMA-aided 6G wireless communication systems," *IEEE Trans. Veh. Technol.*, vol. 72, no. 8, pp. 10659–10670, Aug. 2023.
[40] A. Jeffrey and D. Zwillinger, *Table of Integrals, Series, and Products*, 7th ed. Oxford, U.K.: Academic, 2007.
[41] M. Abramowitz and I. A. Stegun, *Handbook of Mathematical Functions with Formulas, Graphs and Mathematical Tables*. Mineola, NY, USA: Dover, 1972.

Qiang Li (Graduate Student Member, IEEE) received the B.S. degree in communications engineering from Lanzhou University, Lanzhou, China, in 2016. He is currently pursuing the Ph.D. degree with the School of Information and Communication Engineering, Xi'an Jiaotong University, Xi'an, China.

His research interests include information security, covert communication, and NOMA technique.

Mr. Li currently serves as a reviewer for the IEEE JOURNAL ON SELECTED AREAS IN COMMUNICATIONS, IEEE TRANSACTIONS ON VEHICULAR TECHNOLOGY, and IEEE ACCESS.

Dongyang Xu (Member, IEEE) received the Ph.D. degree from the Department of Information and Communication Engineering, Xi'an Jiaotong University, Xi'an, China, in 2019.

He is currently an Associate Professor with the School of Information and Communications Engineering, Xi'an Jiaotong University, and has also been affiliated with Southeast University, Nanjing, China. He has authored 80+ publications including papers in prestigious journal/conferences, such as the IEEE INTERNET OF THINGS JOURNAL, IEEE TRANSACTIONS ON INFORMATION FORENSICS AND SECURITY, IEEE TRANSACTIONS ON INDUSTRIAL INFORMATICS, IEEE TRANSACTIONS ON VEHICULAR TECHNOLOGY, International Conference on Communications (ICC), and Global Communications Conference (GLOBECOM). His research interests include wireless communication, quantum sensing, information security, and machine learning.

Dr. Xu received the Best Paper Rewards from *China Communications* in 2017. He has hosted and participated in more than ten projects. He has also served as the Technical Program Committee Member for IEEE/CIC ICC in China and GLOBECOM. He is a Member of the IEEE Communications Society and the IEEE Vehicular Technology Society.

Keyue Zhang received the B.E. degree in microelectronics and the Ph.D. degree in electronics science and technology from Xi'an Jiaotong University, Xi'an, China, in 2016 and 2023, respectively.

She works as a Postdoctoral Fellow with the School of Electronics and Information, Northwestern Polytechnical University, Xi'an. Her research interests include the study of nonlinear effect mechanisms and suppression methods in microwave millimeter wave devices and circuits.

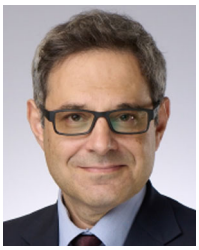

Keivan Navaie (Senior Member, IEEE) received the Ph.D. degree in electronics and computer engineering from Tarbiat Modares University, Tehran, Iran, in 2004.

He is a Chair Professor with Intelligent Networks, School of Computing and Communications, Lancaster University, Lancaster LA, U.K. He concurrently serves as the Principal AI Technology Consultant with the Information Commissioner's Office, U.K. His research encompasses a broad spectrum of domains, including deep learning, privacy-enhancing AI, AI regulations, distributed and federated AI, connectivity resilience in cyber–physical systems and the IoT, as well as applications of machine learning, and artificial intelligence.

Prof. Navaie is a Fellow of the Institution of Engineering and Technology, a Chartered Engineer in the UK, and a Senior Fellow of the Higher Education Academy.

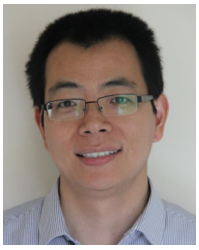

Zhiguo Ding (Fellow, IEEE) received the B.Eng. degree from Beijing University of Posts and Telecommunications, Beijing, China, in 2000, and the Ph.D. degree from Imperial College London, Imperial College London, U.K., in 2005.

He is currently a Professor of Communications with Khalifa University, Abu Dhabi, UAE, and has also been affiliated with Princeton University, Princeton, NJ, USA. His research interests are 6G networks, multiple access, energy harvesting networks, and statistical signal processing.

Dr. Ding recently received the EU Marie Curie Fellowship 2012–2014, the Top IEEE TVT Editor 2017, the IEEE Heinrich Hertz Award 2018, the IEEE Jack Neubauer Memorial Award 2018, the IEEE Best Signal Processing Letter Award 2018, the Friedrich Wilhelm Bessel Research Award 2020, the IEEE SPCC Technical Recognition Award 2021, and the IEEE VTS Best Magazine Paper Award 2023. He is a Distinguished Lecturer of IEEE ComSoc and a Web of Science Highly Cited Researcher in two categories in 2022. He is serving as an Area Editor for the IEEE TRANSACTIONS ON WIRELESS COMMUNICATIONS, and IEEE OPEN JOURNAL OF THE COMMUNICATIONS SOCIETY; an Editor for IEEE TRANSACTIONS ON VEHICULAR TECHNOLOGY; and was an Editor for IEEE WIRELESS COMMUNICATION LETTERS, IEEE TRANSACTIONS ON COMMUNICATIONS, and IEEE COMMUNICATION LETTERS from 2013 to 2016.